SOME ASPECTS OF THE YIELDING AND FLOW OF LITHIUM FLUORIDE

by

RIHO HANS MARTINSON

A THESIS SUBMITTED IN PARTIAL FULFILMENT
OF THE REQUIREMENTS FOR THE DEGREE OF
MASTER OF APPLIED SCIENCE
IN THE DEPARTMENT
OF
METALLURGY

We accept this thesis as conforming to the
standard required from candidates for
the degree of MASTER OF APPLIED SCIENCE

Members of the Department
of Metallurgy

THE UNIVERSITY OF BRITISH COLUMBIA
February 1963

In presenting this thesis in partial fulfilment of the requirements for an advanced degree at the University of British Columbia, I agree that the Library shall make it freely available for reference and study. I further agree that permission for extensive copying of this thesis for scholarly purposes may be granted by the Head of my Department or by his representatives. It is understood that copying or publication of this thesis for financial gain shall not be allowed without my written permission.

Department of Metallurgy

The University of British Columbia,
Vancouver 8, Canada.

Date March 13, 1963

ABSTRACT

Tension tests have been performed on LiF single crystals. The results of strain rate change tests are not wholly consistent with current theories of deformation processes. The number of mobile dislocations appears to depend sensitively on the stress prevailing during straining.

A short investigation of the effect of removing surface layers during deformation was undertaken. The surfaces of chemically polished LiF single crystals are not sites of strong work-hardening.

The effects of magnesium-rich surface layers on the mechanical properties of LiF have been studied. The yield stress, critical tensile stress, and work-hardening slope increase linearly with layer thickness, while the strain to fracture decreases rapidly with increasing layer thickness. The results of tension tests, supplemented by metallographic evidence, indicate that the yield stress and the critical tensile stress are not determined by surface source operation.

ACKNOWLEDGEMENT

The author thanks his research directors, Dr. E. Teghtsoonian and Professor W. M. Armstrong for their advice and encouragement. Stimulating discussions with fellow graduate students aided in the clarification of many points. Thanks are due to Messrs. R. G. Butters and R. J. Richter for technical assistance. Special thanks are extended to Mr. W. R. Irvine for his many helpful suggestions and for the loan of equipment.

Financial assistance was provided by The Steel Company of Canada, Limited in the form of The Stelco Graduate Fellowship in Metallurgy, and by The National Research Council under Grant #A-1463. Both awards are gratefully acknowledged.

TABLE OF CONTENTS

TABLE OF CONTENTS CONTINUED

FIGURES

FIGURES CONTINUED

INTRODUCTION

The mechanical properties of LiF are, at present, understood in greater detail than those of any other material. A recent series of elegant experimental investigations by J.J. Gilman and W.G. Johnston has yielded detailed quantitative information regarding the behaviour of individual dislocations in both strained and unstrained LiF -- information which is currently exerting a profound influence on the development of a general microscopic plasticity theory. Since the work of Gilman and Johnston is described in numerous readily available reviews[1-3] and original communications[4-13], it will not be surveyed here.

However, in spite of this intensive and fruitful study, certain fundamental aspects of the plasticity of LiF remain obscure. For instance, one question awaiting a satisfactory resolution is: Does the nucleation and/or multiplication of dislocations in LiF occur preferentially near the crystal surface? It is known[1] that mobile dislocation half-loops are readily introduced into LiF by surface damage and that the mechanical properties of LiF are affected by such surface damage. However, it is not known whether in the absence of large numbers of artificially introduced surface sources, dislocations arise more easily near the crystal surface than in the crystal interior. It is also not known to what extent existing mobile dislocations multiply preferentially near the crystal surface. A study of the influence of alloyed surface layers on the mechanical properties of LiF was undertaken in order to answer these questions.

Fundamental differences exist between the work-hardening theories proposed for LiF[9], and those currently thought to apply to face-centered cubic metals. In view of this, it seemed desirable to perform certain standard experiments on LiF -- the Cottrell-Stokes behaviour of copper, for instance, is commonly rationalized in terms of the interaction of mobile dislocations with barriers possessing long-range stress fields. The behaviour of individual dislocations in strained LiF[7] suggests that static barriers possessing long-range stress fields either do

not exist or do not strongly impede the motion of dislocations, at least not in the early stages of plastic flow. The existence of a Cottrell-Stokes law in LiF would therefore imply that the current interpretation of Cottrell-Stokes behaviour is not unique.

One reason why the macroscopic plastic properties of ionic crystals have not been studied in the same detail as those of metals is that it has long been thought difficult to perform adequate mechanical tests on non-metallic crystals. The simple tension test has frequently been eschewed in principle because of "the inherent difficulty of performing tensile tests on brittle materials". Instead, recourse is often had to bend tests with an attendant uncertainty in stress and a non-uniformity of strain. It is part of the purpose of the present work to show that it is possible to perform adequate tensile tests on LiF with only moderate precautions. Any irreproducibility in strength properties is shown to be attributable to random variations in testing procedure which, at least in principle, apply equally well to tensile tests on metallic crystals.

PREVIOUS WORK

Recent reviews of the effects of environments (solid, liquid, and gaseous) on the mechanical properties of crystals are available.[14,15] It will suffice to state here that the observed effects are many and varied, not always internally consistent in the light of current theories, and that a classification of the fundamental effects according to the following scheme has recently been proposed:[15]

(1) The dislocation egress effect -- a barrier to the egress of dislocations from the crystal provided by, say, a solid surface film may be expected to influence the mechanical properties of crystals.

(2) The surface drag effect -- a screw dislocation intersecting a clean surface has a slip-step associated with it. As the screw dislocation moves under applied stress, a new surface is formed at the slip-step. A change in surface energy or a mechanical barrier to the formation of new surface may be expected to influence the mechanical properties of crystals.

(3) Dislocations may be anchored at the surfaces of crystals by:

(a) selective etching to produce hollow dislocations.[16]

(b) solute pinning effects.

(c) selective precipitation of impurities on dislocations.

The surface anchoring effect may be detectable in measurements of the critical resolved shear stress if surface sources are important in determining the critical resolved shear stress.

(4) The force field effect -- a change in the elastic constants or lattice parameters near a crystal surface may influence the course of deformation by causing an elastic interaction with the strain fields of dislocations moving near the surface.[17,18]

Any observed effect of environment on the mechanical properties of crystals may be regarded as a superposition of these four fundamental effects. Only (2)[19,20] and (4)[17] have been analysed (semi-quantitatively); a resolution of

an observed effect into its components is therefore virtually impossible at present.

A short investigation of the effect of magnesium-alloyed surface layers on the deformation of LiF single crystals has been published by A.R.C. Westwood.[21] The relevant conclusions from this research are:

(1) Metallographic evidence shows that surface coatings can act as barriers to the egress of edge dislocations from the LiF crystal.

(2) Tests on as-cleaved, chemically polished, coated and uncoated specimens show that a coating can restrict the operation of artifically introduced surface sources, thereby raising the yield stress. A coating also decreases the initial rate of work-hardening of as-cleaved LiF crystals by reducing the number of active dislocation sources, so that mutual dislocation interference effects are lessened.

(3) A catastrophic break-through of groups of edge-dislocations piled up against the coating can cause stress drops in the stress-strain curve.

(4) A surface coating can act as a stable barrier to the egress of dislocations, causing pile-up, coalescence, and the formation of crack-nuclei beneath the film. This can reduce the stress and strain to fracture of coated crystals to half that of uncoated crystals.

EXPERIMENTAL PROCEDURE

(1) Material

Two LiF crystals (A and B) were purchased from The Harshaw Chemical Company, Cleveland, Ohio, in the form of cleaved rectangular blocks, approximately 1 x 1 x 1 inches in dimension. No analysis was available from the supplier, however, it proved possible to estimate the impurity content by comparing the mechanical properties of A and B with those of other crystals obtained from the same source.

(2) Specimen preparation

(i) Cleaving

Rods of the nominal dimensions 2.5 x 2.5 x 25 mm were cleaved from the as-received crystals using the apparatus shown in Fig. 1.

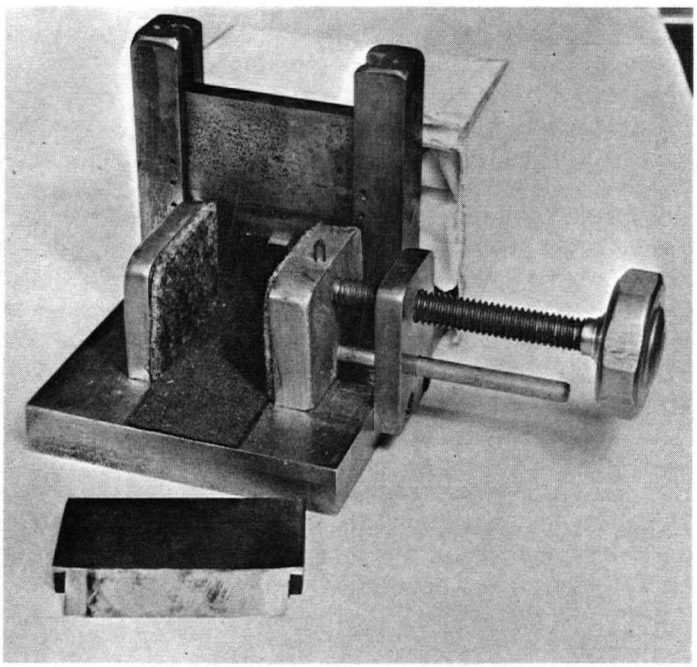

Fig. 1. Cleaving Apparatus

Prior to cleaving, a grid was scribed onto one face of the as-received crystals with a tool-maker's surface gauge in order to facilitate the maintenance of constant specimen dimensions.

(ii) Annealing

The as-cleaved specimens were annealed for 24 hours at 600°C in air. During annealing, the specimens were supported on high density 99.9% alumina platens. The annealing furnace was cooled at the mean rate of 50°C per hour.

(iii) Polishing

All specimens were chemically polished before testing. Two polishing treatments were used (Fast and Slow).

Fast -- The crystal was rotated at approximately $\frac{1}{2}$ rps. in 50% HBF_4. This treatment removed material at the rate of 38 μ per minute.

Slow -- A standard cycle was employed, consisting of:

(a) Immersion of the specimen in 50% HF for 1 minute, rinsing and drying, and

(b) Rapid rotation in a 2 vol. % aqueous NH_4OH solution for 4 minutes. The stirring speed was critical, optimum surface appearance resulting from a stirring speed of the order of 10 rps.

The Slow polishing treatment removed 1.4μ per minute from the crystal surface.

During polishing operations, the crystals were mounted on a glass rod with a drop of "Pyeseal". The rod was rotated at the required rates by a portable stirring motor.

In all cases, at least 25 μ was polished off the surfaces of as-annealed crystals before the crystals were either coated or tested.

(iv) Etching

The standard dislocation etching reagents for LiF were slightly modified for this investigation. The approximate compositions of the two etches (A and W) used were:

Etch A -- Equal parts of conc. HF and glacial CH_3COOH plus 1 vol. % conc. HF

saturated with $FeCl_3$.

Etch W -- A 2×10^{-4} molar solution of $FeCl_3$ in distilled water.

The exact optimum concentrations of the reagents were found by trial and error for individual crystals. The Fe^{3+} concentration required in Etch A was especially critical.

The specimens were rinsed in ethyl alcohol and dried in a warm air stream between individual polishing and etching operations.

It was found that polishing in HBF_4 did not usually produce a surface amenable to etchpitting. The surface structure resulting from HBF_4 polishing could, however, be removed quickly by polishing in the NH_4OH solution. It was ascertained that the surface structure resulting from HBF_4 polishing did not affect the mechanical properties of the specimens.

(v) Production of evaporated coatings

Evaporated magnesium coatings were produced in a bell jar, using the geometry shown in Fig. 2.

The magnesium strip (approximately $\frac{1}{8} \times 0.01$ in. in cross-section) was wound onto frames as shown and was heated by the passage of an electric current. The strip was cleaned in dilute HCl, rinsed in alcohol, and dried immediately prior to sealing off the apparatus. During the evaporation process, each specimen was supported near the axis of the frame by a wire to which it had been attached with "Pyeseal". The evaporation process was carried out in a vacuum of 2×10^{-4} mm of Hg, produced by a mechanical fore pump and an oil diffusion pump.

As it proved impossible to control accurately the amount of magnesium deposited on the specimens, the following standard procedure was employed which maximized it:

(1) The auto-transformer controlling the input to the main step-down transformer was preset to give an output of approximately 50 volts.

(2) Power was applied instantaneously to the step-down transformer.

(3) The evaporation process was allowed to continue until it was terminated

either by local failure of the magnesium strip, or by a short circuit caused by magnesium deposited on the alumina rods of the supporting frame.

The amount of magnesium deposited on each specimen was assessed by weighing.

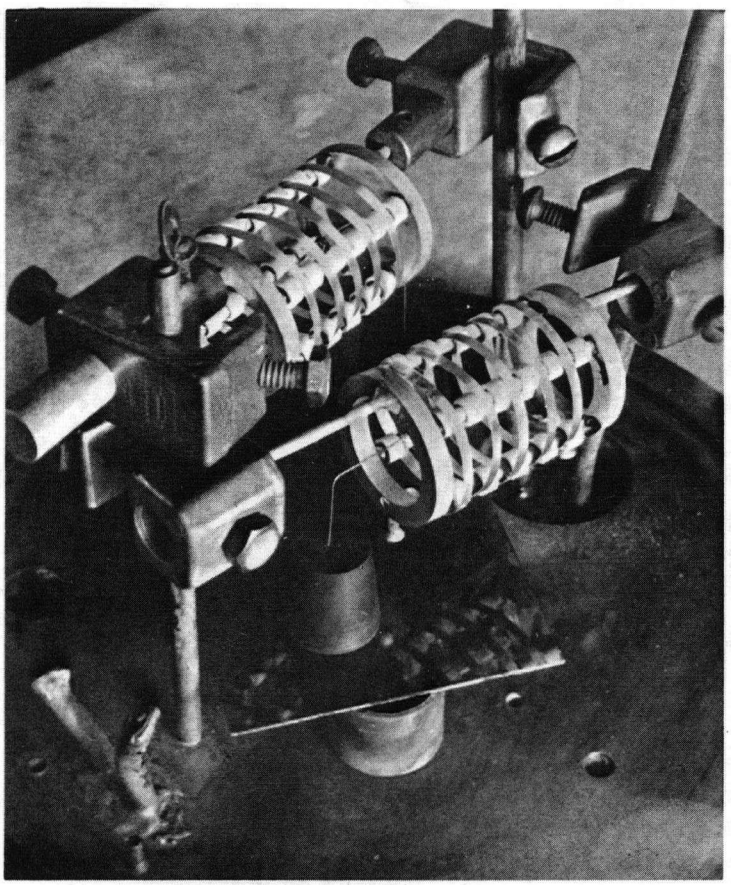

Fig. 2. Geometry during evaporation of magnesium.

(vi) Diffusion

After a satisfactory magnesium coating had been produced, the specimens were sealed off under vacuum in Pyrex vials as shown in Fig. 3. A carbon sheath was used to prevent the possibility of a chemical reaction between the magnesium and Pyrex.

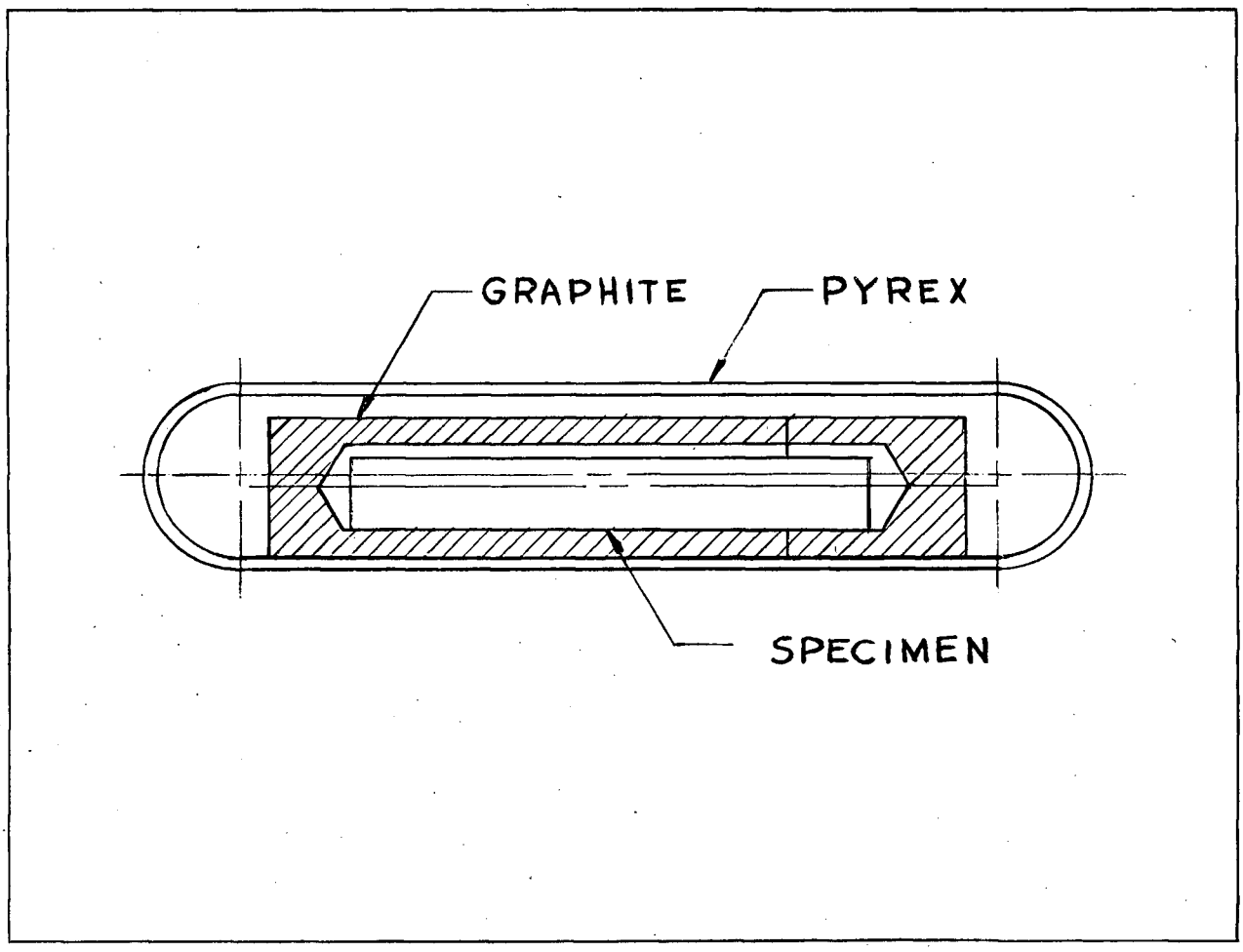

Fig. 3. Longitudinal section of a diffusion vial.

Efforts were made to reduce the oxygen partial pressure in the diffusion vials by alternately pumping and back-filling with tank nitrogen. Before the vials were sealed, a final pumping reduced the total gas pressure to approximately 2×10^{-3} mm of Hg.

The majority of diffusion runs were made in two identical tube furnaces whose temperatures were controlled to within $\pm$ 1°C by calibrated Chromel-Alumel thermocouples driving Minneapolis-Honeywell controllers. A check of the temperature of each run was obtained from an independent, calibrated Chromel-Alumel thermocouple placed in contact with the diffusion vials inside the furnace tube.

Because of their high specific heats, the furnaces cooled quite slowly when the power was shut off at the end of a diffusion run. A furnace cooling curve from 500°C is shown in Fig. 4.

After diffusion, the specimens were rinsed in approximately 0.1 M HCl for 30 seconds in order to remove adherent portions of the MgF_2 layer produced during diffusion annealing.

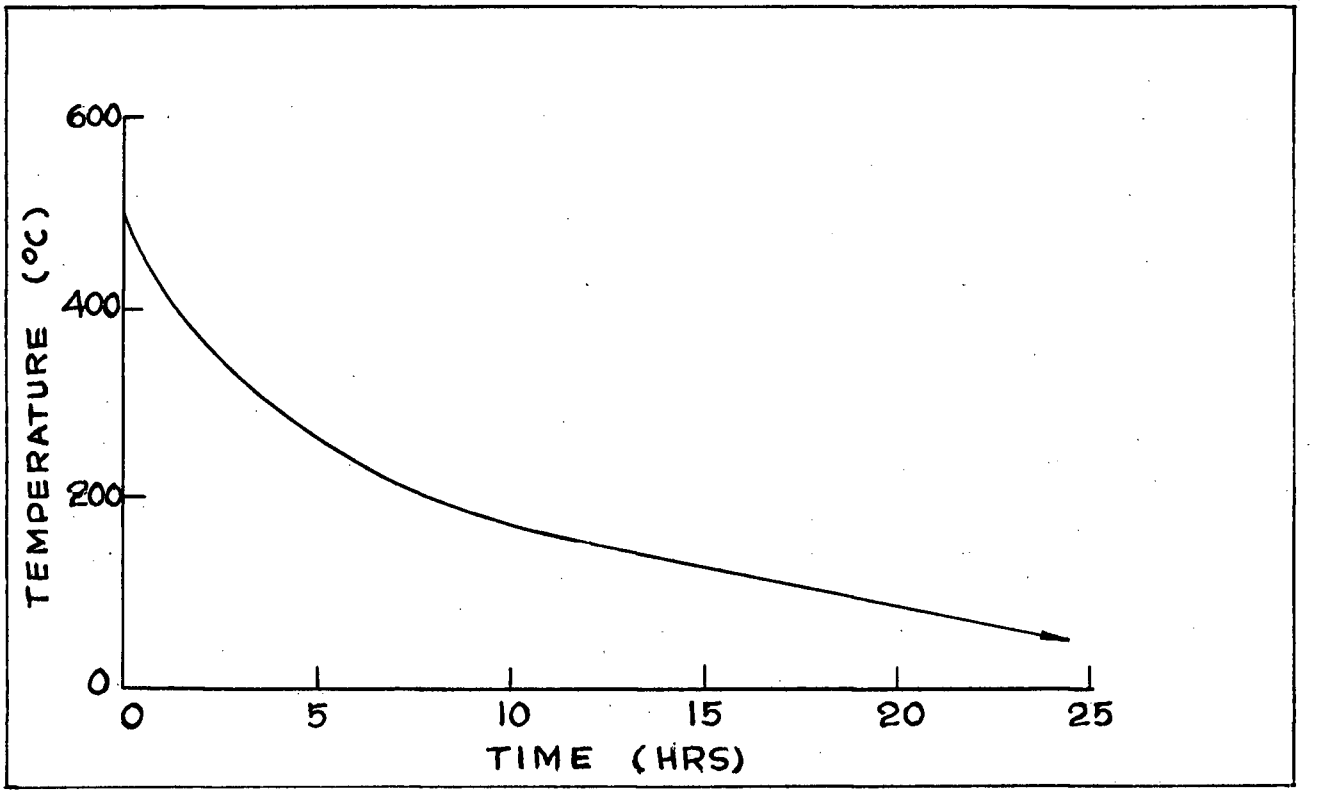

Fig. 4. Cooling curve of furnace #1.

(3) Testing procedures

(i) Mounting

The specimens were mounted in mild steel grips of the design shown in Fig. 5. A commercially available epoxy resin (Epon 828 plus Curing Agent D, marketed by The Shell Chemical Company, and mixed according to directions) was used to bond the specimens to the grips. The epoxy was cured at approximately 95°C in a water bath, the total curing cycle requiring 90 minutes per end mounted.

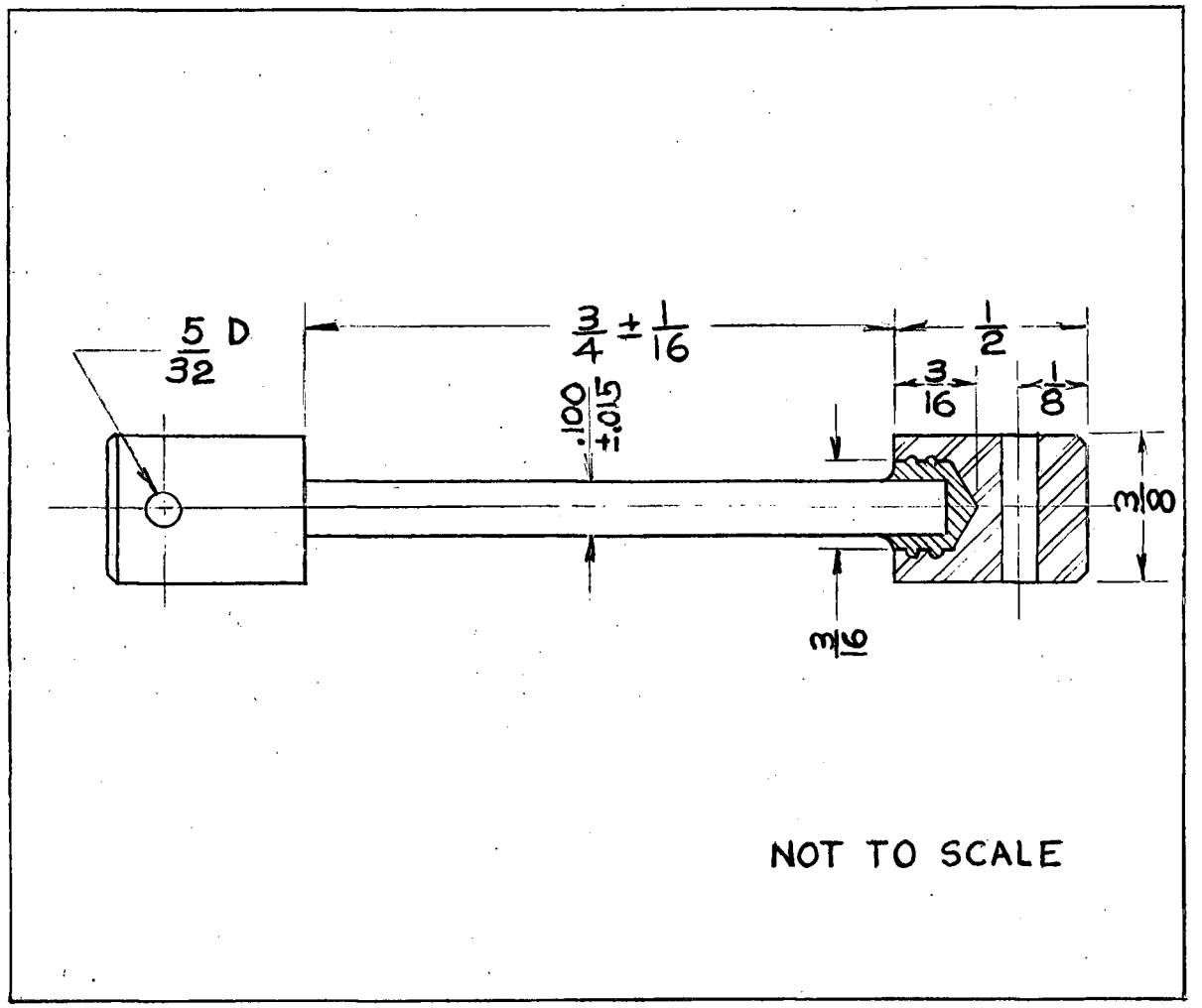

Fig. 5. Longitudinal section of mounted specimen.

During mounting, the specimens and the grips were supported in a special jig to ensure axial alignment of the grips and reasonably central positioning of the specimen relative to the grips. Shims were sometimes used to correct the position of the specimens relative to the grips.

Specimen dimensions were measured after mounting, by a Gaertner travelling microscope accurate to 1 μ . Two measurements were usually made of each dimension.

(ii) Tensile testing.

All tensile tests were performed on two Instron mechanical testing machines, models TT-B. A universal gripping arrangement previously described[22] was used in order to minimize bending moments on the specimens caused by non-central positioning of the specimens during mounting.

A majority of the tensile tests performed during the course of this investigation were done on a machine which did not incorporate a "quick-change" crosshead speed changer. It was necessary to change gears manually between speed changes; the process requiring approximately 40 seconds. A "quick-change" modification enables the speed change to be effected in approximately 1 second, during which time certain transient effects exist in the motion of the crosshead. A detailed account of the procedures used to effect the changes in crosshead speed may be found in the Experimental Results section.

A preliminary investigation of the effect of surface removal on the mechanical properties of LiF was made. The procedures used were:

(1) The specimen was strained a given amount and removed from the testing machine.

(2) The specimen, complete with grips, was rotated slowly in conc. HBF_4 for a given time.

(3) The specimen was replaced in the machine, care being taken that it was replaced in the same position relative to the universal grips as previously.

The specimens subjected to polishing during the test were also polished in HBF_4 prior to mounting, and were generally given a second short (20 sec.) HBF_4 polish immediately before being tested.

(iii) Metallography

A Reichert metallographic microscope (model MeF) and a Reichert petrographic microscope were used for metallographic observations and observations of birefringence respectively.

(iv) Microhardness measurements.

All coated specimens were sectioned longitudinally after testing and etched in order to determine the thickness of the magnesium-rich layer. Microhardness traverses were made across the diffused layers on a group of specimens in order to assess the strength properties of the layers.

The microhardness profiles were obtained using a Tukon hardness tester with a Knoop diamond pyramid indenter. The indentations were made with the long diagonal of the indenter positioned along the $\langle 100 \rangle$ direction parallel to the edge of the specimen. A 5 gram load was used to produce most of the indentations.

Each data point on the plotted profiles represents the mean of three measurements on each of four indentations. The individual indentations in a group of four were no closer than three times the long diagonal of each indentation.

It did not prove possible to perform adequate microhardness measurements on diffused layers thinner than 20 μ.

EXPERIMENTAL RESULTS

(I) Uncoated crystals

(i) Quality of the specimens:

Metallographic examination of annealed and polished specimens showed the following:

(1) The grown-in dislocation density was between 5×10^4 and 1×10^5 dislocations per cm^2, excluding dislocations in subgrain boundaries.

(2) The mean subgrain size was 2 mm. Most of the subgrains were equiaxed; some very narrow subgrains whose boundaries lay in (110) planes were, however, occasionally observed near the ends of the specimens.

(3) Cleavage steps were very small (approximately 1 μ high) and were well rounded off.

(4) No evidence of micro-cracks or other damage was found at the corners of polished specimens.

(5) The specimen faces were usually parallel to within 10 μ.

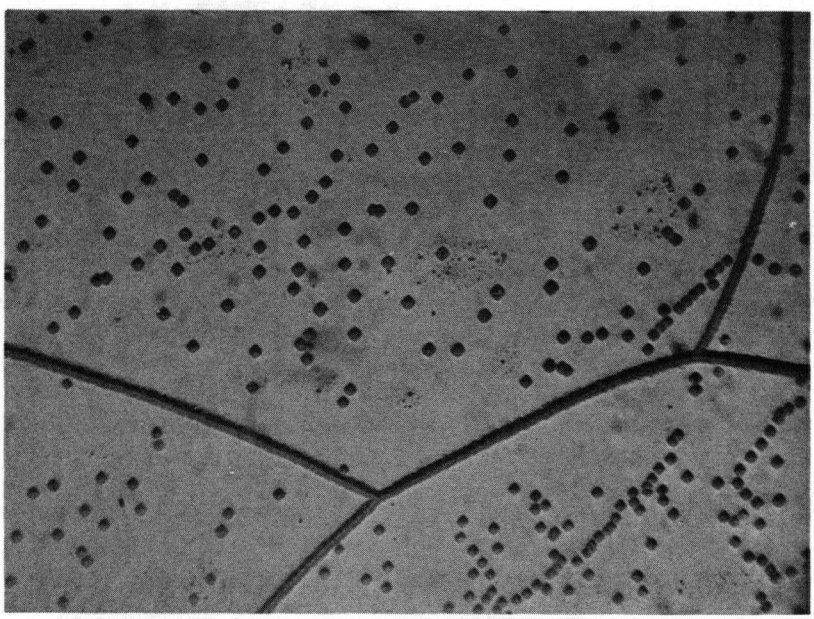

Fig. 6. Grown-in dislocation structure in LiF.
Etch-pit density = $4.0 \times 10^4/cm^2$. Magnification - 110 X

End damage in the form of large cleavage steps and short transverse cracks often occurred on cleaving these relatively slender specimens. The damage was, however, confined to regions which were immersed in the epoxy during mounting and thus did not affect the quality of the specimens within the gauge length.

It did not prove possible to control the specimen dimensions more closely than to approximately $\pm$ 0.2 mm. This variation in specimen dimensions proved troublesome in that it caused a certain non-axiality in the loading in the very early stages of plastic flow. The use of shims during mounting compensated to some extent for this dimensional variation.

(ii) Tensile tests

The parameters obtained from the load-elongation curves are defined in Fig. 7.

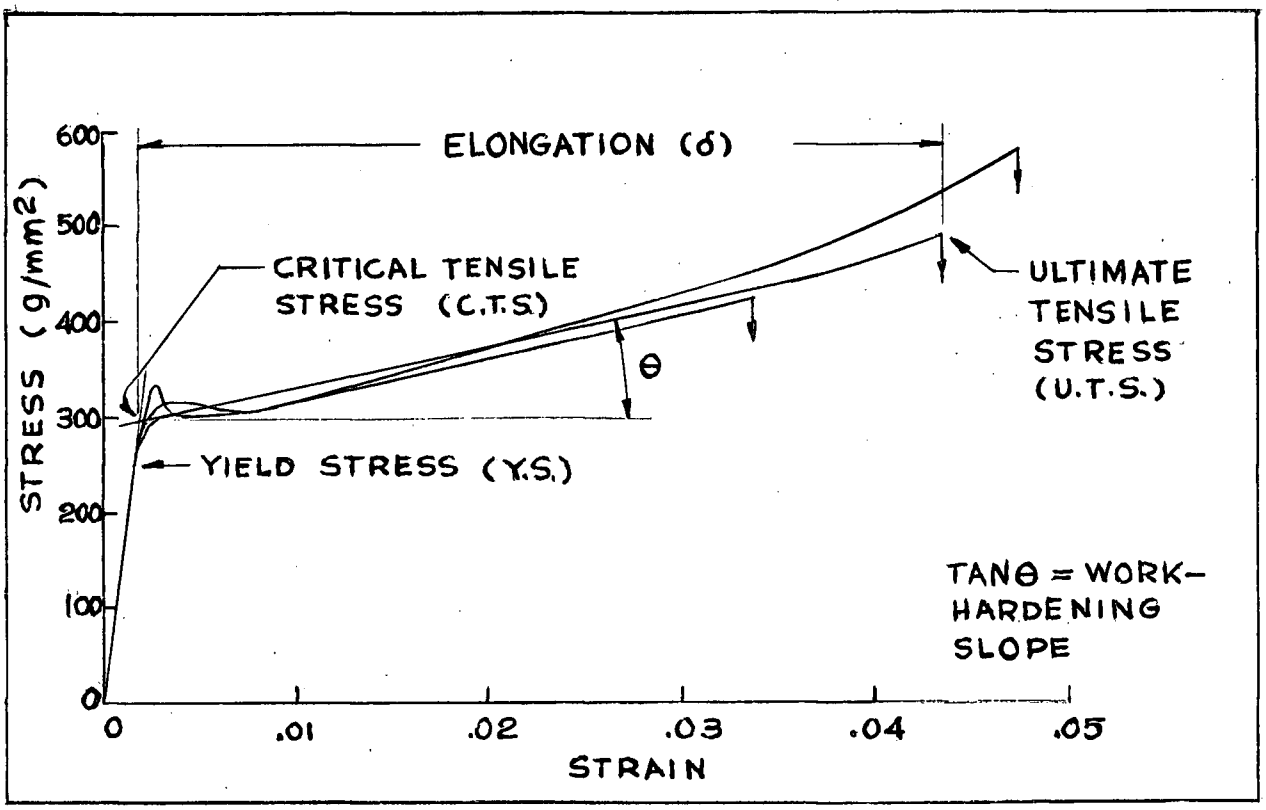

Fig. 7. Typical stress-strain curves.

The appearance of the initial region of the load-elongation curves varied from specimen to specimen -- typical curves are shown in Fig. 7. The strain to fracture also varied greatly; total tensile strains between 3% and 13% being observed. The results of simple tension tests on uncoated crystals are tabulated in Appendix II.

An attempt was made to assess the mechanical properties of the epoxy by mounting a steel rod in the grips and performing a tensile test on it. The relevant observations are:

(1) The elastic modulus of the epoxy was so small that it alone determined the slope of the elastic portion of the stress-strain curve. After corrections for machine deflection had been applied, the as-measured Young's modulus of the rod was approximately 5 times lower than the true value.

(2) Slipping of the epoxy-metal bond did not start until loads in excess of 25 lbs. were applied.

At a strain-rate of 4.3×10^{-4} sec^{-1}, systematic differences appear between the average* properties of specimens prepared from crystals A and B as shown in Fig. 8.

	Y.S. (g/mm^2)	C.T.S. (g/mm^2)	Θ (g/mm^2)	δ (%)
Crystal A	305 ± 19	385 ± 30	$6.8 \pm 1.5 \times 10^3$	3.8 ± 0.8
Crystal B	254 ± 18	295 ± 6	$4.4 \pm 0.4 \times 10^3$	4.3 ± 0.7

Fig. 8. Summary of the mechanical properties of crystals A and B. Strainrate -- 4.3×10^{-4} sec^{-1}

* The standard deviation is used as a measure of error throughout this thesis.

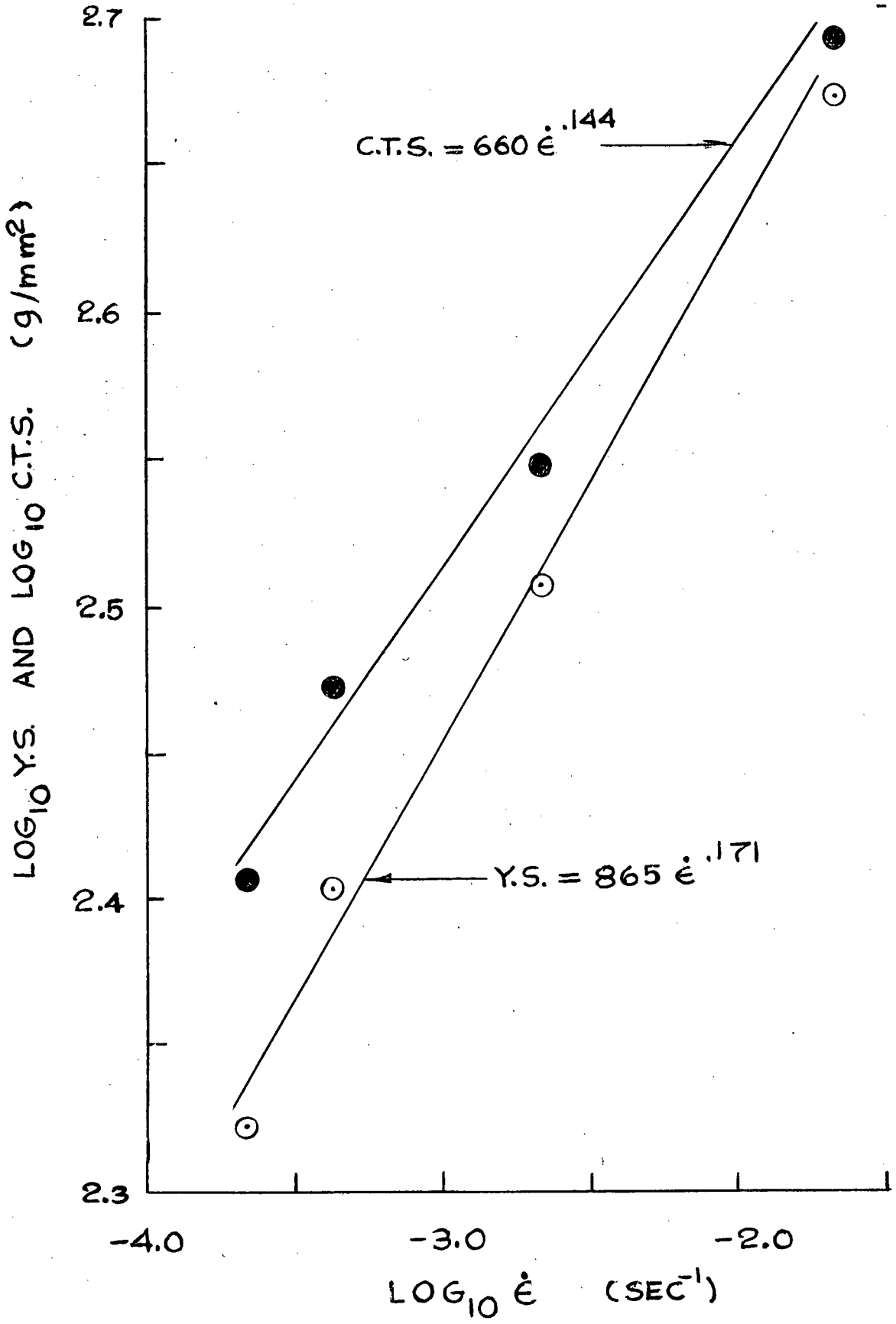

Fig. 9. Log-log plot of the initial strength properties versus strain rate.

The variation of the initial strength properties of crystal B with strain-rate is shown in Fig. 9. No systematic variation of work-hardening rate with strain-rate was observed.

Fracture occurred by cleavage along the (100) plane normal to the axis of tension, generally near the middle of the gauge length. Very ductile crystals (those exhibiting more than 7% elongation) always fractured near the grips. Usually the fracture surfaces were plane, showing no detail except small cleavage steps. In three instances it was observed that in addition to the cleavage crack causing failure, several smaller cleavage cracks in the neighbourhood of the main crack had been nucleated and had begun to propagate across the specimen. These arrested cracks seemed to have originated on or near the crystal surface.

(iii) Birefringence observations

Slip occurred on all of the four equally stressed $\{110\}\langle 110\rangle$ slip systems from the beginning of plastic flow, subject to the following two general observations:

(1) Usually, slip occurred predominantly on the planes (011) and (0T1) for a portion of the gauge length and on (101) and (T01) for an adjacent portion.

(2) Unusually ductile crystals slipped predominantly on two orthogonal slip planes along the whole gauge length.

Strong birefringence bands were in all cases observed in the immediate vicinity of the grips. Kink bands were occasionally observed in extremely ductile crystals.

(iv) Strain-rate change tests

Strain-rate change tests were conducted according to three different procedures:

Procedure I -- The specimen was extended, at a strain-rate $\dot{\epsilon}_1$, to a strain ϵ_1; the crosshead motion was stopped, and the load was allowed to relax for a time t, where 20 sec. $< t <$ 30 sec. The specimen was then extended at a strain-rate

$\dot{\epsilon}_2$ to a strain ϵ_2, and the process was repeated until the specimen fractured.

Procedure II -- The same procedure as I was used, except that $t = 1$ second.

Procedure III -- The crystal was extended at a strain rate $\dot{\epsilon}_1$ to a strain ϵ_1, the crosshead motion was then reversed until only a few grams of the load remained on the specimen. A time $t \approx 150$ sec. was allowed to elapse, after which the specimen was extended at a strain rate $\dot{\epsilon}_2$.

Typical stress-strain curves obtained from strain rate change experiments are shown in Fig. 14. Graphs of $\Delta\sigma$ and $\frac{\Delta\sigma}{\sigma}$ as functions of σ are shown in Fig. 15, Fig. 16, Fig. 17, Fig. 18. Graphs of $\Delta\sigma'$ versus σ obtained when no changes in strain-rate are made are shown in Fig. 19.

(v) Surface removal during interrupted tensile tests

The effect of removing a 76 μ surface layer by chemical polishing at various points on the stress-strain curve is illustrated in Fig. 20.

It is apparent that the work-hardening slope is not changed by the polishing treatment, but that the flow stress is changed discontinuously by an amount $\Delta\sigma''$ which varies linearly with the flow stress .

(vi) Removal of surface layers during strain rate change tests

The effect of removing 76 μ and 38 μ surface layers during strain rate change tests is shown in Fig. 21 and Fig. 22.

The change in the flow stress is irreversible by an amount $\Delta\sigma'''$ which varies with strain and with the amount of material removed. It should be realized that this is an irreversibility of a second kind since the strain rate changes were conducted according to Procedure III, which does not produce an irreversible effect of the first kind, as may be seen from Fig. 19.

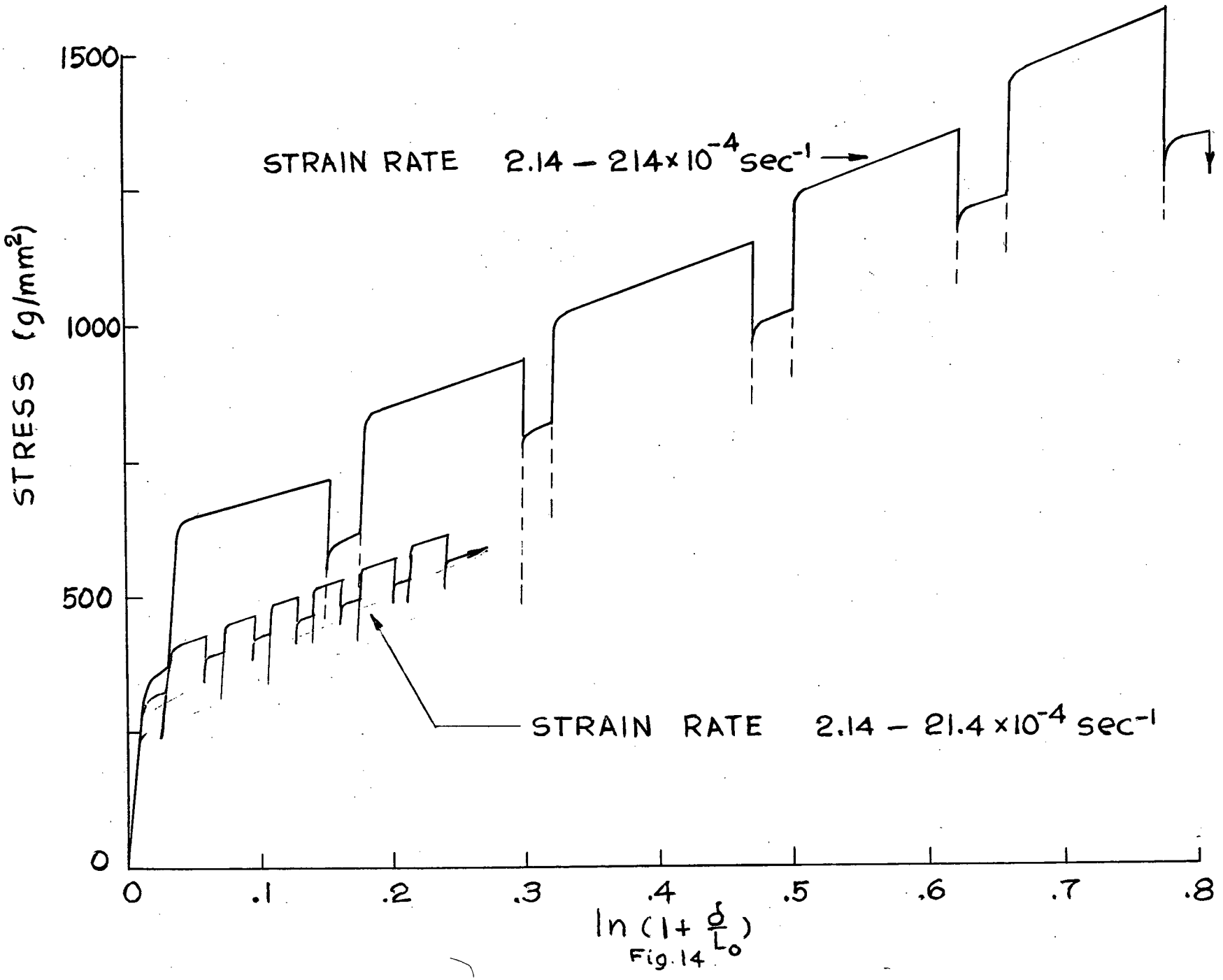
1500
1000
500
0
STRESS (g/mm²)
STRAIN RATE 2.14 – 214×10⁻⁴ sec⁻¹
STRAIN RATE 2.14 – 21.4×10⁻⁴ sec⁻¹
0
.1
.2
.3
.4
.5
.6
.7
.8
ln (1 + δ/L₀)

Fig. 14

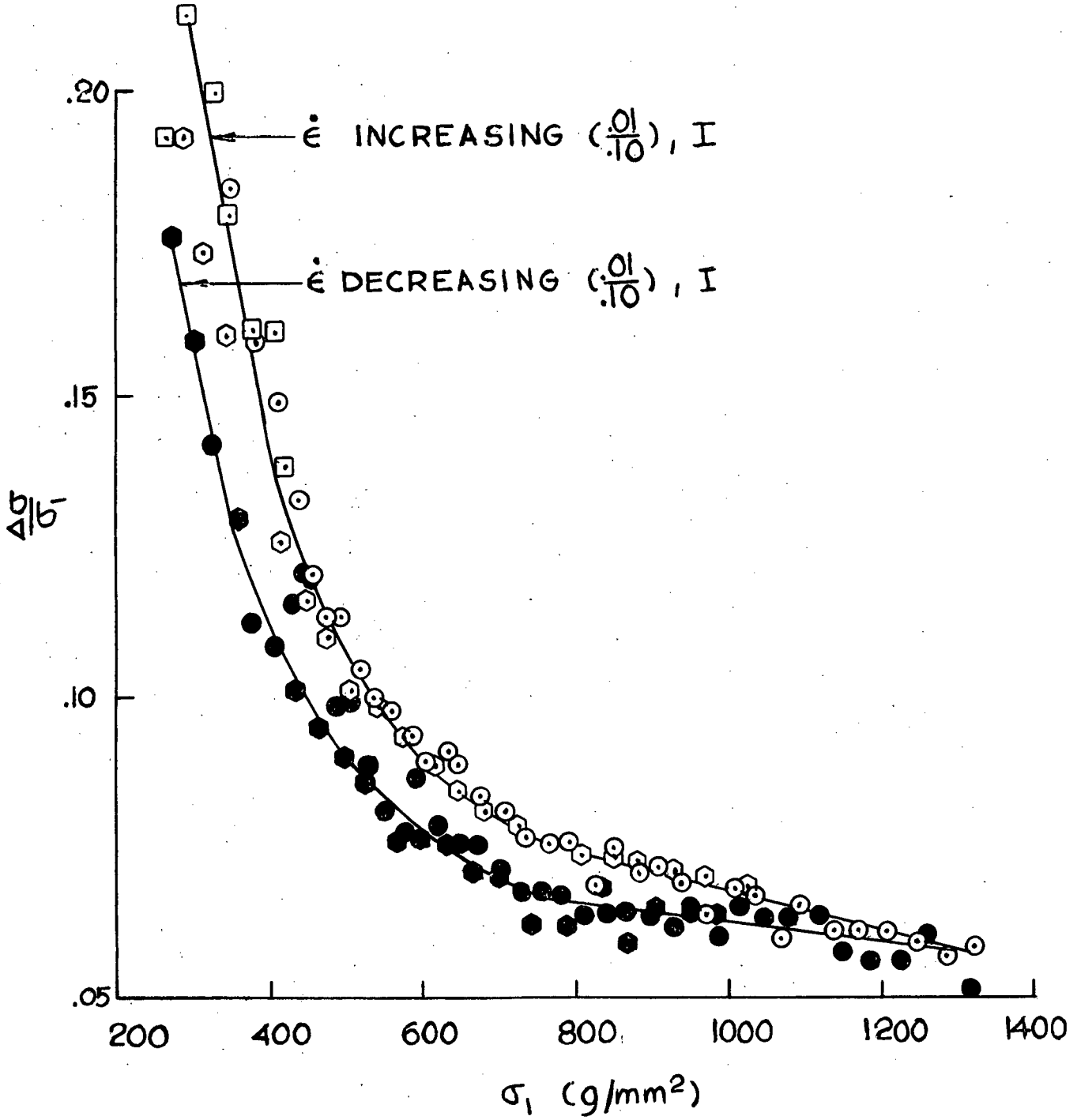

Fig. 15. Results of 10:1 strain rate change experiments. Strain rate cycled between 2.28×10^{-4} sec^{-1} and 22.8×10^{-4} sec^{-1}

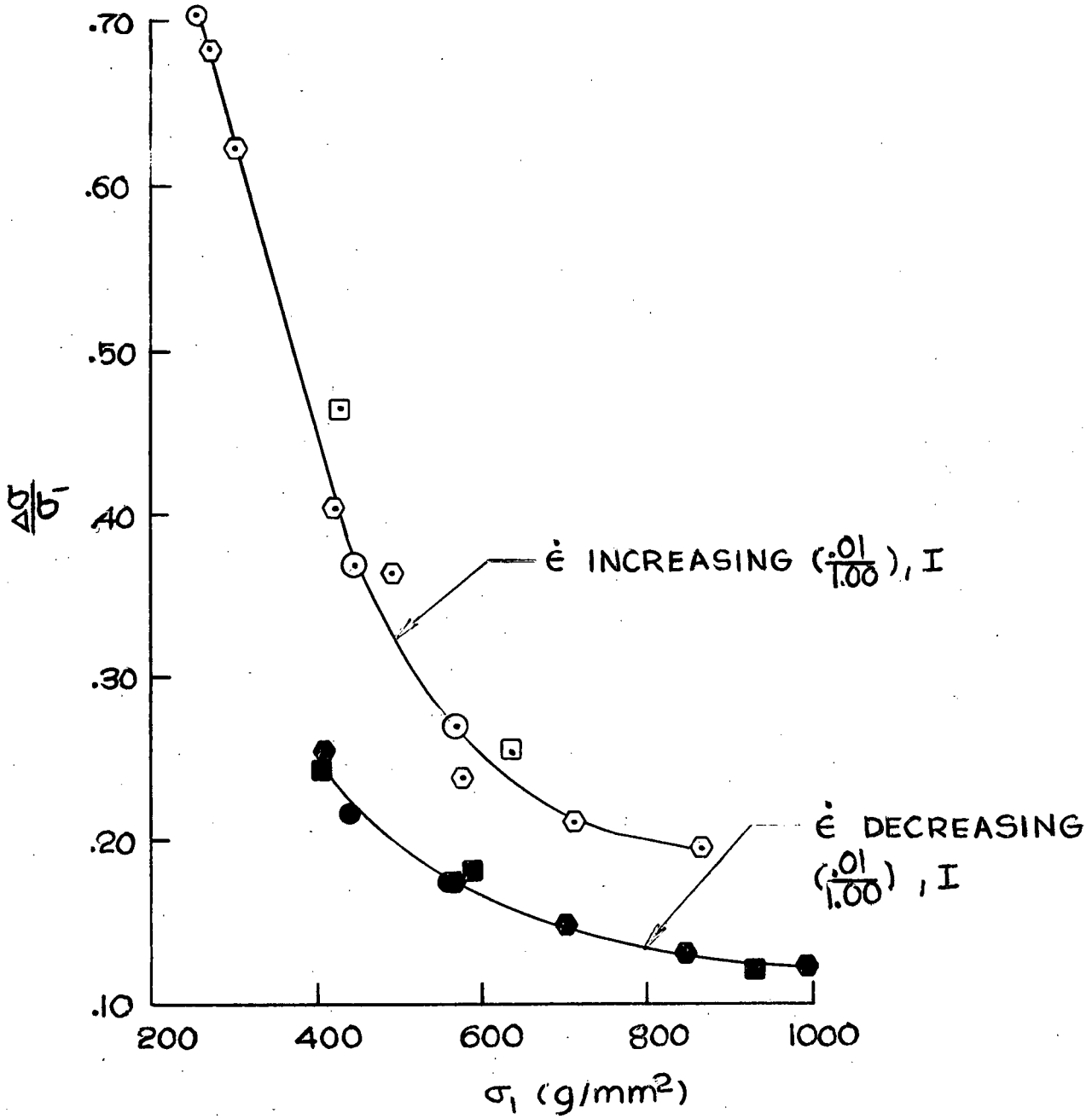

Fig. 16. Results of 100:1 strain rate change experiments. Strain rate cycled between 2.14×10^{-4} sec^{-1} and 214×10^{-4} sec^{-1}

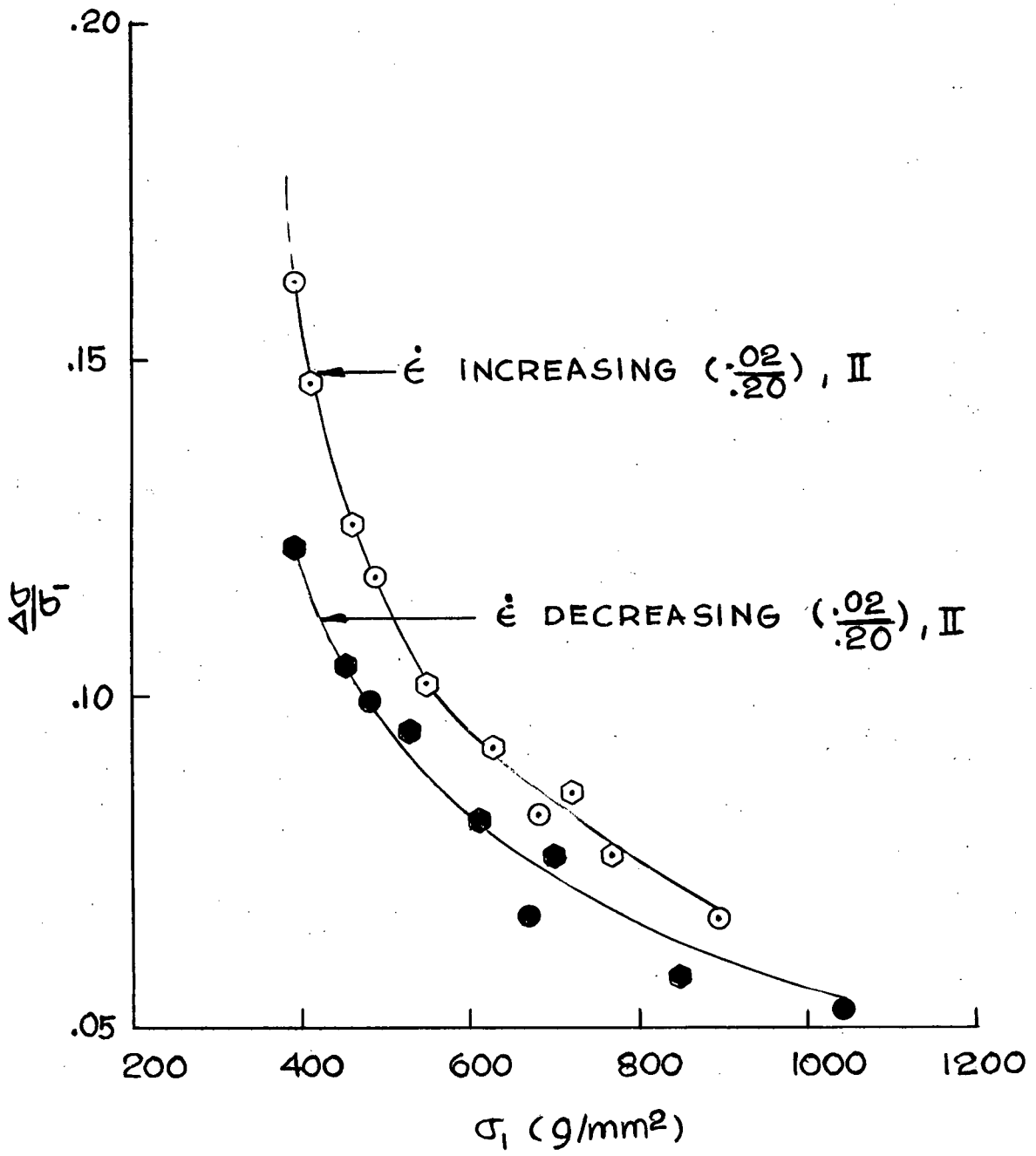

Fig. 17. Results of 10:1 strain rate change experiments. Strain rate cycled between 4.28×10^{-4} sec^{-1} and 42.8×10^{-4} sec^{-1}

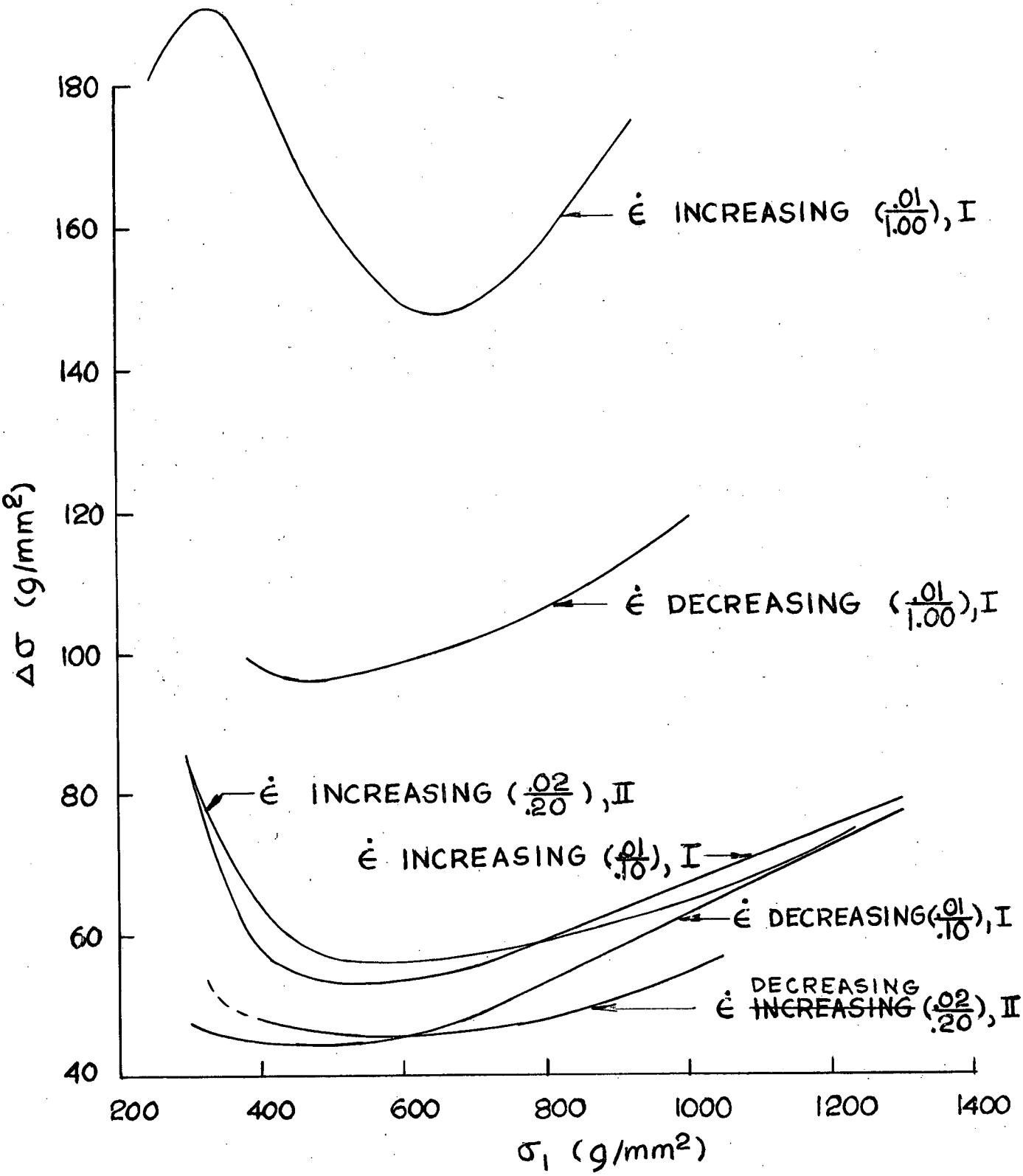

Fig. 18. Smoothed plots of $\Delta\sigma$ versus σ_1

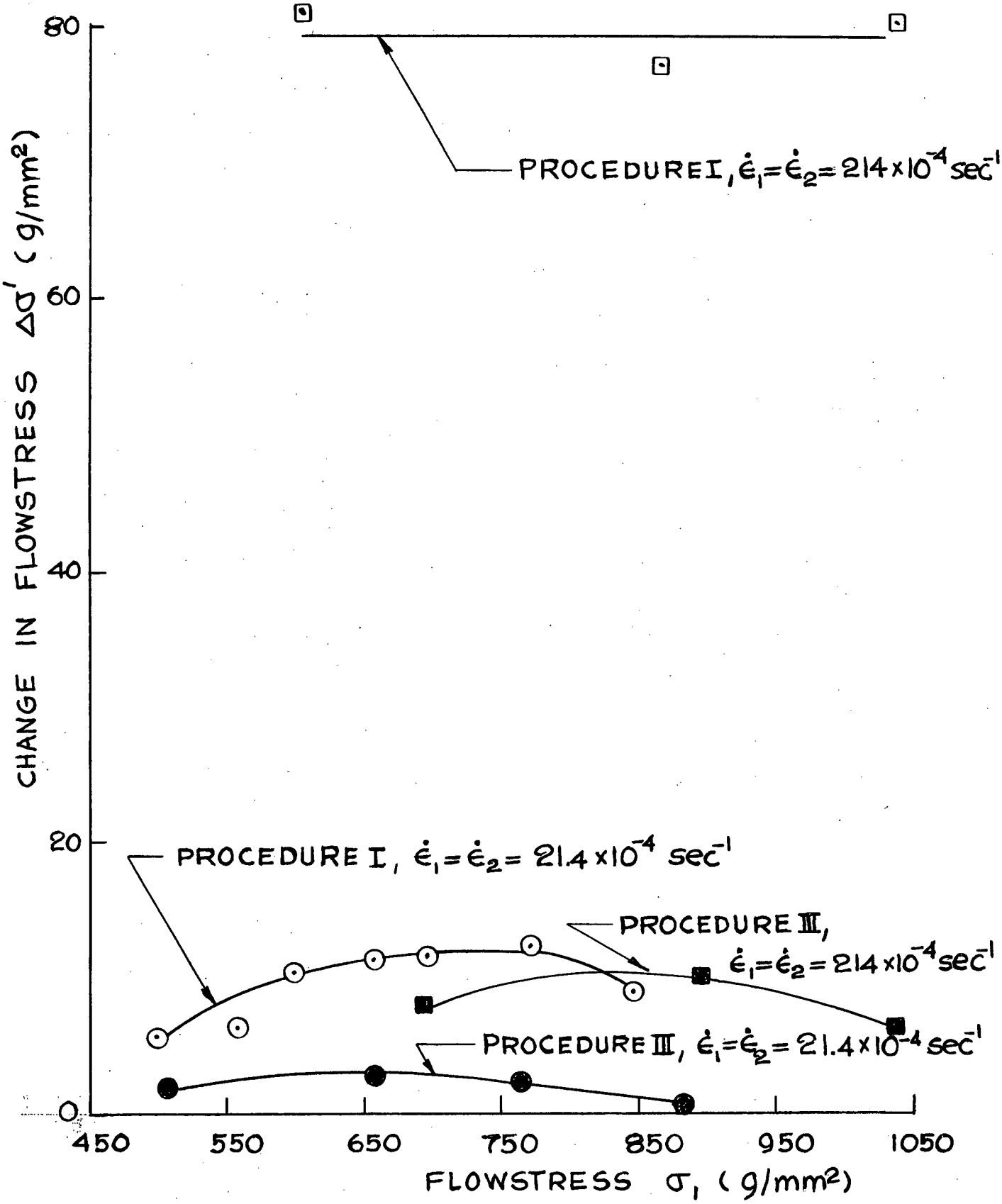

Fig. 19. Strengthening observed in LiF during interrupted tension tests.

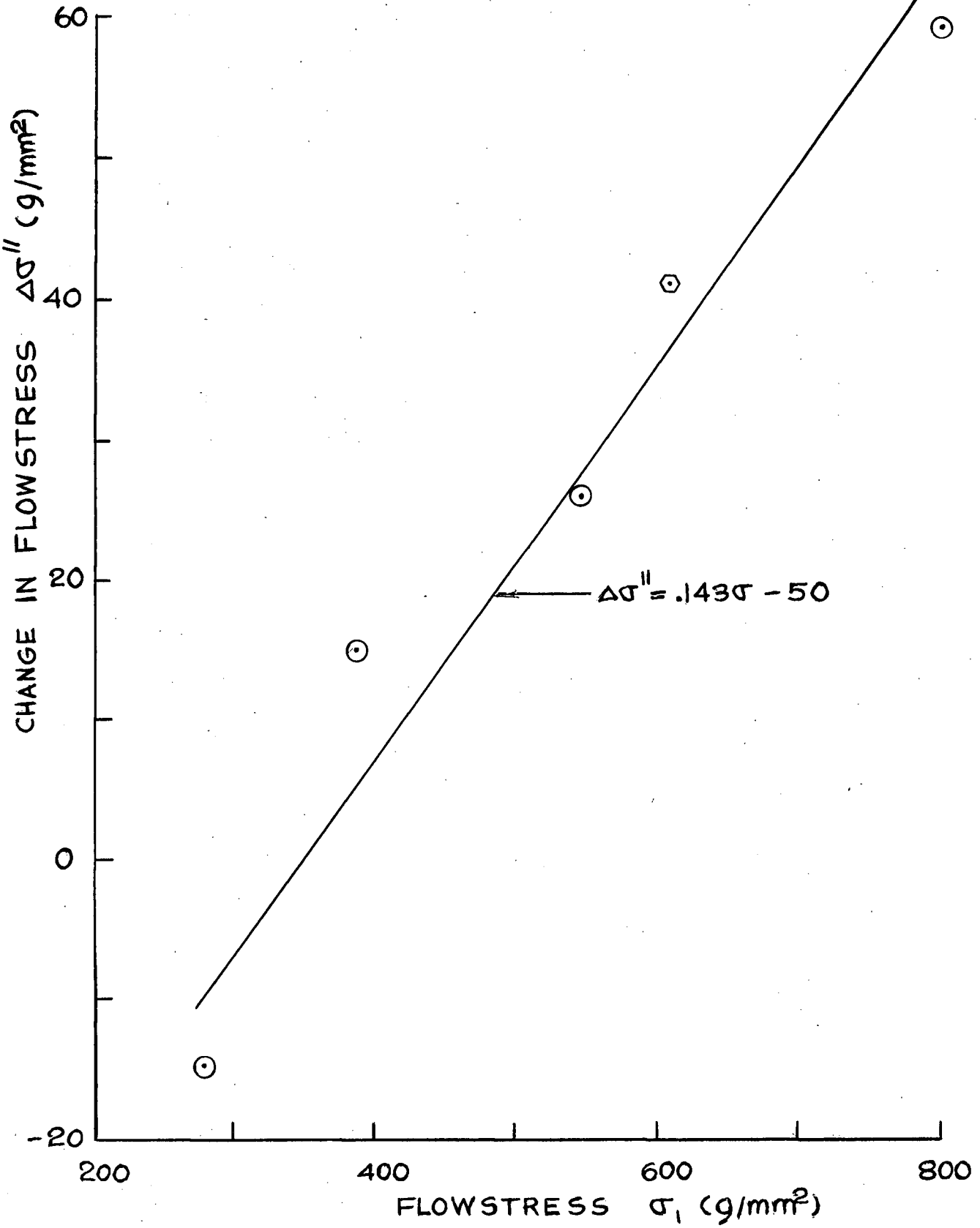

Fig. 20. Change in flow stress induced by removing a 76 μ surface layer during tension testing. Strain rate - 4.28×10^{-4} sec^{-1}

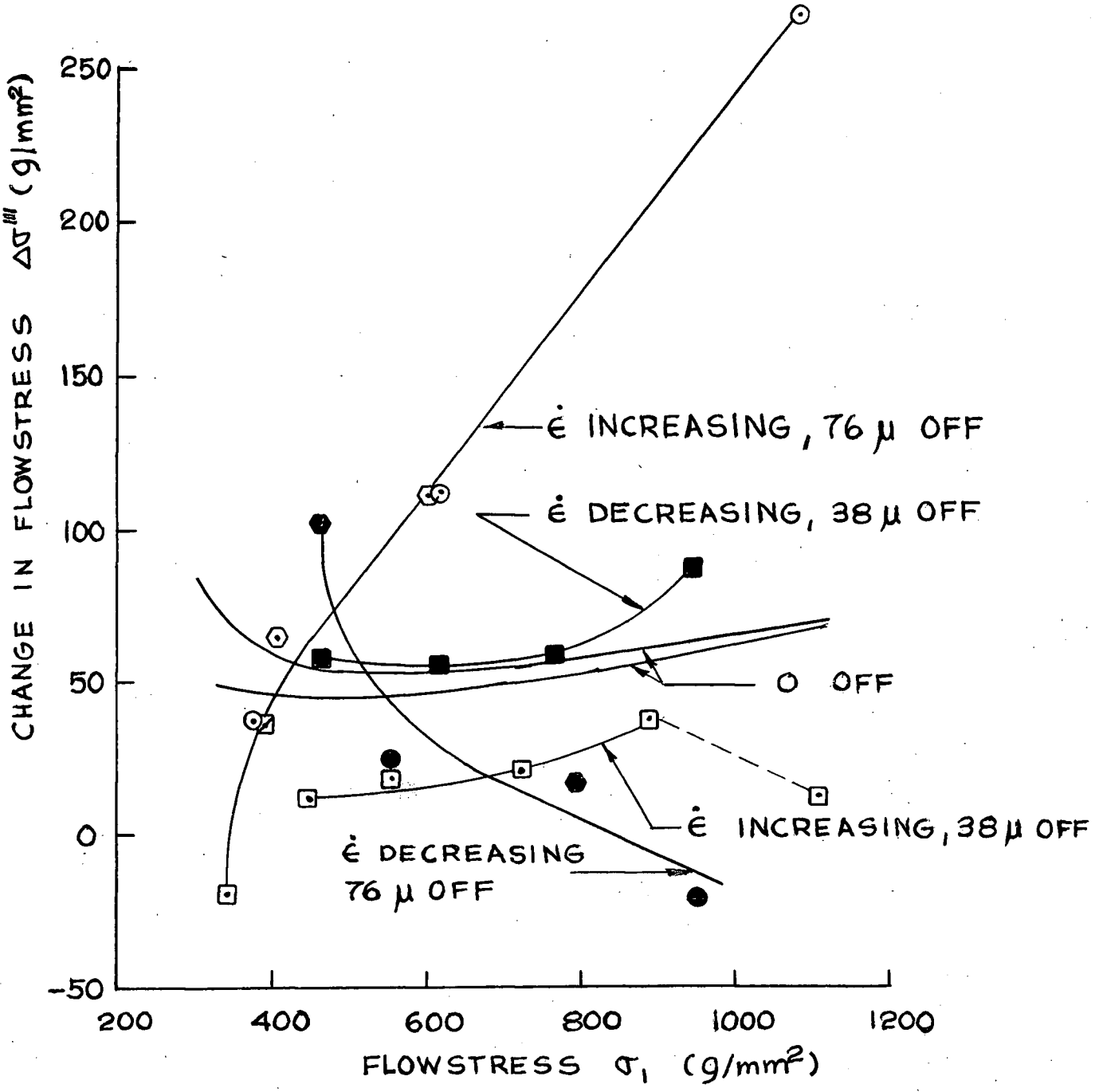

Fig. 21. Effect of removing surface layers during 10:1 strain rate change experiments. Strain rate cycled between 2.14×10^{-4} sec^{-1} and 21.4×10^{-4} sec^{-1}

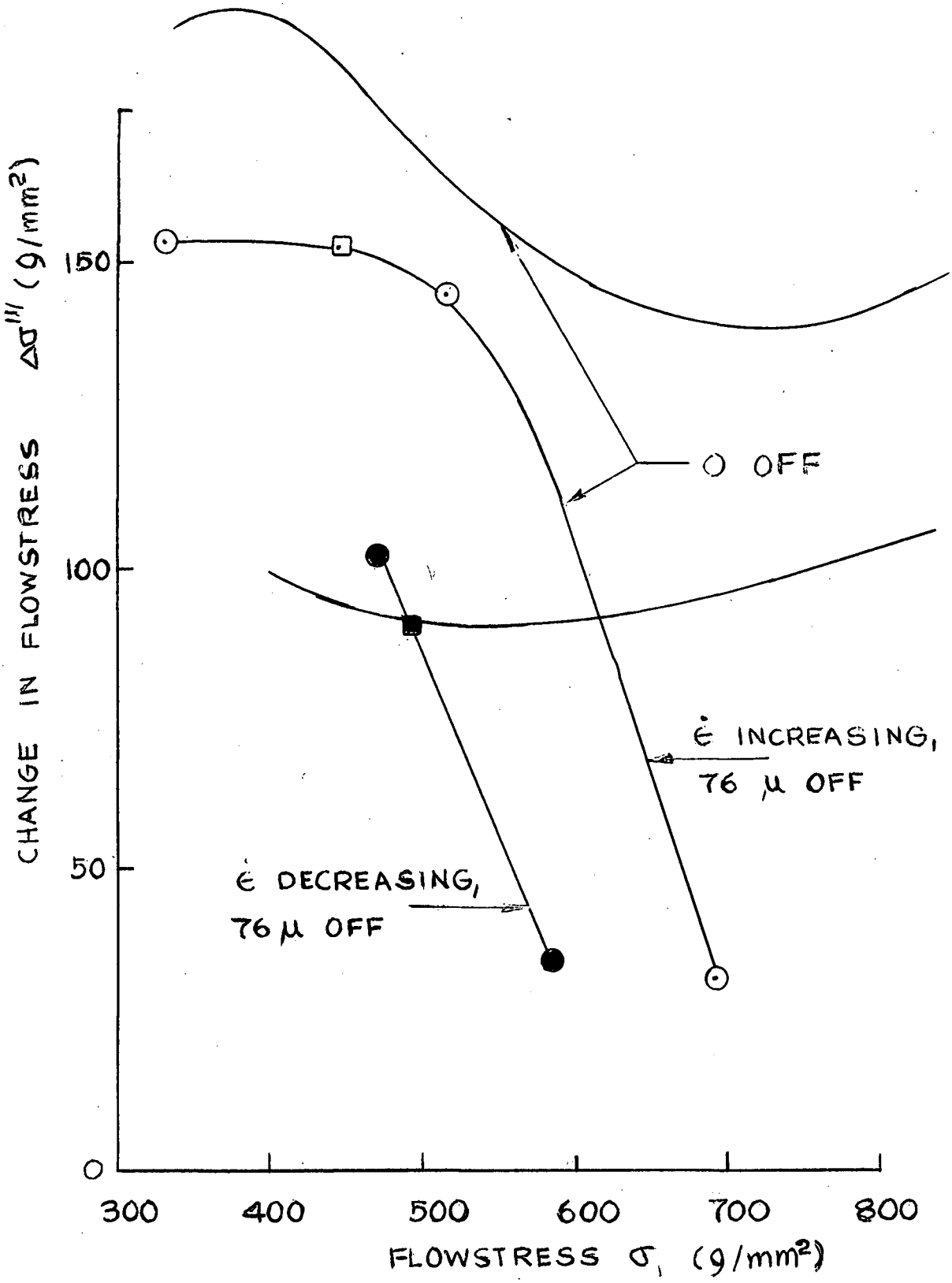

Fig. 22. Effect of removing surface layers during strain rate change experiments. Strain rate cycled between 21.4×10^{-4} sec^{-1} and 214×10^{-4} sec^{-1}

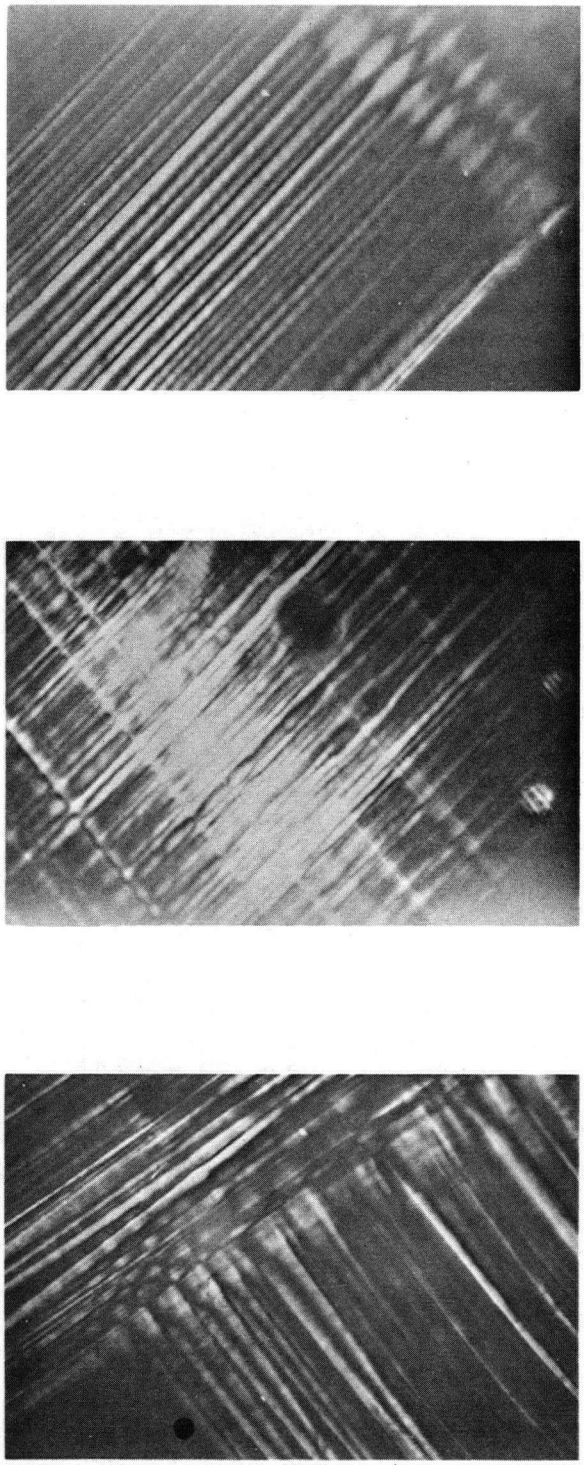

Fig. 23. Birefringence in uncoated crystals 50X

Summary of experimental observations for uncoated specimens.

(1) The yield stress and critical tensile stress of LiF containing approximately 5 ppm. magnesium vary with strain rate according to the equations:

$$Y.S. = 660\,\dot{\epsilon}^{.171}$$

$$C.T.S. = 865\,\dot{\epsilon}^{.144}$$

where

$$2.14\times10^{-4}\ sec^{-1} \leq \dot{\epsilon} \leq 214\times10^{-4}\ sec^{-1}$$

(2) The initial work hardening rate is substantially independent of strain rate in the above range of strain rate.

(3) LiF does not obey the Cottrell-Stokes law with respect to strain rate changes; the plot of $\Delta\sigma$ versus σ exhibiting a minimum. The approximately linear portion of the $\Delta\sigma$ versus σ curve extrapolates to a non-zero $\Delta\sigma$ at $\sigma = 0$.

(4) The change in flow stress of LiF as measured according to procedures I and II is irreversible by an amount that increases with the absolute value of the faster strain rate. The amount of irreversibility is closely equal to the change in the flow stress induced by aging under load for 45 seconds, for both 10:1 and 100:1 changes in strain rate.

(5) The amount of irreversibility in the change of flow stress becomes negligibly small if the strain rate change is conducted according to procedure III.

(6) The change in flow stress caused by polishing 76 μ off the crystal surface is $\Delta\sigma''$, where:

$$\Delta\sigma'' = .143\,\sigma - 50$$

(7) During 1:10 strain rate change tests, the effect of removing material from the surface of the specimen is to cause an irreversibility of the second kind to appear in the flow stress which:

(a) increases with increasing stress

(b) increases with the amount of material removed.

(8) During 100:1 strain rate change tests, the effect of polishing off the crystal surface is:

(a) the same for $\Delta\sigma'''_{\uparrow}$ as for $\Delta\sigma'''_{\downarrow}$

(b) such as to decrease $\Delta\sigma'''$ uniformly.

(II) COATED CRYSTALS

(i) Properties of as-evaporated coatings.

The as-evaporated magnesium appeared lustrous and "silvery" at the magnesium-crystal interface, whereas the magnesium-air interface appeared dull and greyish. The amount of magnesium deposited on the specimens varied from approximately 1 milligram to 3 milligrams. All the crystals were completely covered with magnesium in the evaporation process, although no way was found to assess the uniformity of the as-evaporated coatings. Evidence that the coating on any one specimen was, in fact, sufficiently uniform will be presented later.

(ii) Properties of diffused coatings.

After diffusion, the MgF_2 excess magnesium coatings which had formed as a consequence of the reaction between the magnesium and LiF were brown in colour. The degree of adherence of the MgF_2 coating to the substrate varied from specimen to specimen and from place to place on any one specimen. Usually, most of the coating spalled off in large patches on removal of the specimen from the diffusion vial. The remainder was loosened in dilute HCl as described previously. Gas evolution was often observed to accompany the HCl treatment.

No discoloration of the Pyrex vial was observed when the specimens were completely enclosed in the graphite sheaths, although evidence of a reaction between the glass and the magnesium to form MgO was found in certain early runs during which the specimens were not completely protected.

Debye-Sherrer X-ray diffraction patterns of typical as-diffused coatings showed the following:

(1) The as-diffused coatings consisted of MgF_2. Faint magnesium lines were observed in one instance.

(2) The lattice parameters of the as-diffused coatings were identical with those of pure MgF_2 within experimental error (~~0.05 Å~~ 0.005 Å).

(iii) Properties of the surface layers.

Laue X-ray diffraction patterns of selected specimens with thick diffused layers (150 μ) did not appear essentially different from patterns obtained from pure LiF crystals. In particular, Debye rings were not observed in the patterns obtained from crystals with magnesium-rich surface layers.

Debye-Sherrer diffraction patterns of powder ground from the surface of a specimen with a thick (150 μ) diffused layer were successfully indexed as pure LiF patterns. No lattice parameter change greater than 0.005Å was observed and no extra lines appeared.

No second phase was observed by focussing a microscope slightly below the surfaces of crystals with thick diffused layers.

The etching behaviour of the diffused surface layer is shown in Fig. 32 ~~23~~. It should be noted that the photo-micrographs show longitudinal sections of deformed crystals. The "thickness" of the diffused layer is as defined in Fig. 32 ~~23~~.

The diffused surface layers were usually uniform in thickness to within 5% of the layer thickness, and sensibly equal in thickness on both sides of the sectioned crystal. The etching response of the layers did not suggest that the character of the layer on any one crystal varied from one position to another.

It did not prove possible to control the thickness of the diffused layers accurately by varying the duration and/or temperature of the diffusion runs. No correlation between the amount of magnesium deposited on the crystals and the thickness of the diffused layers was established. The measured layer thicknesses as well as corresponding times and temperatures of diffusion are tabulated in Appendix V ~~IV~~.

Micro-hardness profiles of typical diffused layers are shown in Fig.24.

The profiles have been normalized so that the micro-hardness of "pure" LiF is unity. No systematic differences were observed between the micro-hardnesses of crystals A and B.

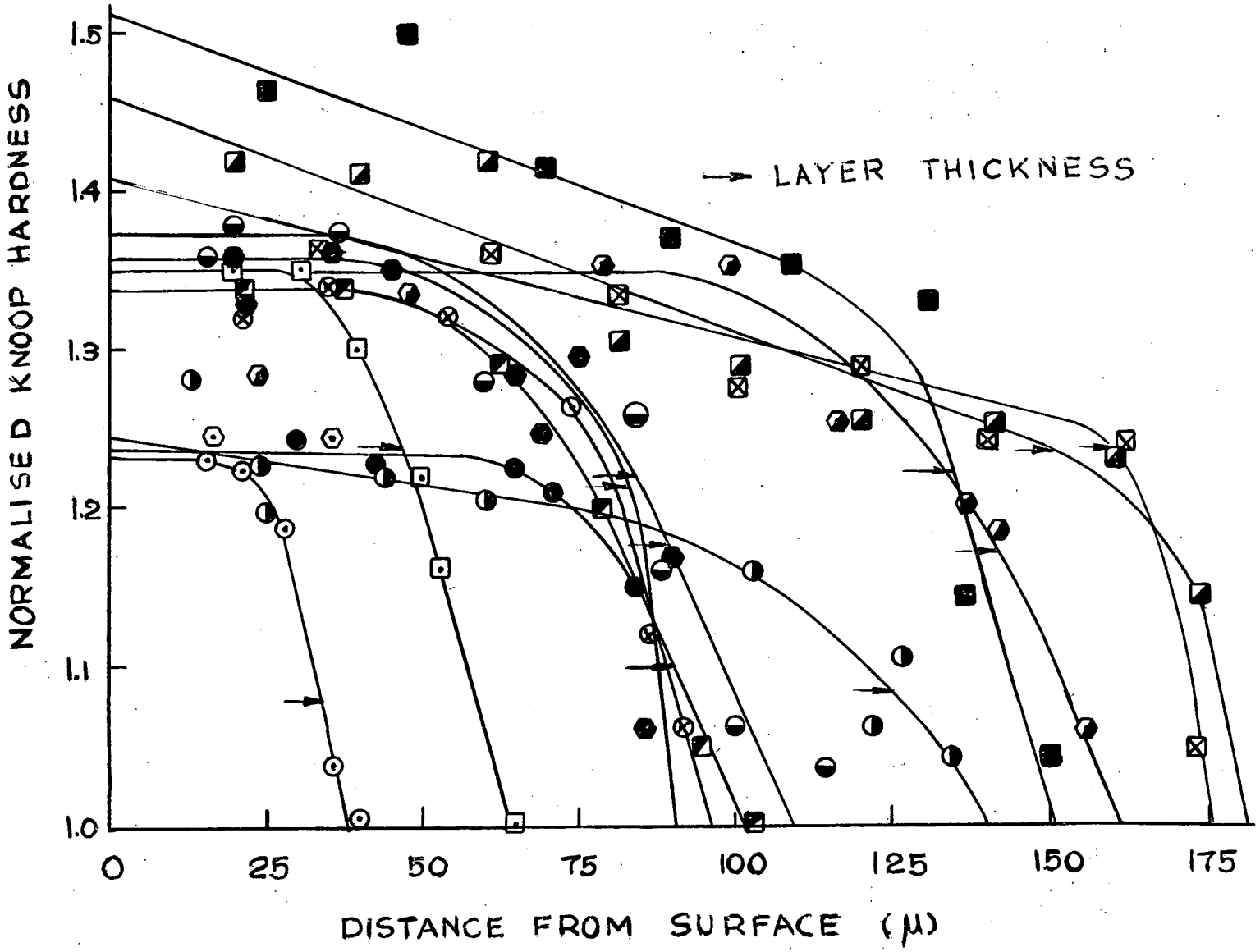
NORMALISED KNOOP HARDNESS
1.5
1.4
1.3
1.2
1.1
1.0
0
25
50
75
100
125
150
175
DISTANCE FROM SURFACE (μ)
LAYER THICKNESS

Fig. 24

The quality of the micro-hardness indentations is shown in Fig. 25.

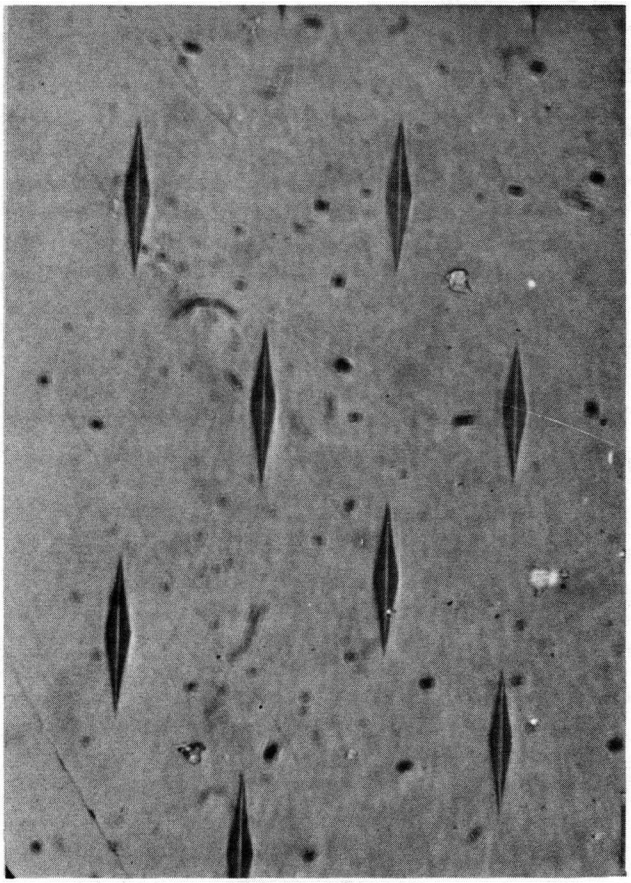

Fig. 25. Micro-hardness indentations in LiF. 720X

(iv) Tensile properties of coated crystals

The variation of the yield stress and the critical tensile stress of surface-alloyed crystals with the thickness of the alloyed layer is shown in Fig. 26 and Fig. 27. The properties of three surface-alloyed crystals which had been abraded ~~on~~ an equal amount (20 strokes) on 4/0 emery paper are also shown in the figures.

Typical stress-strain curves for coated crystals are shown in Fig. 28. No stress drops or yield drops were observed in the stress-strain curves of the coated crystals.

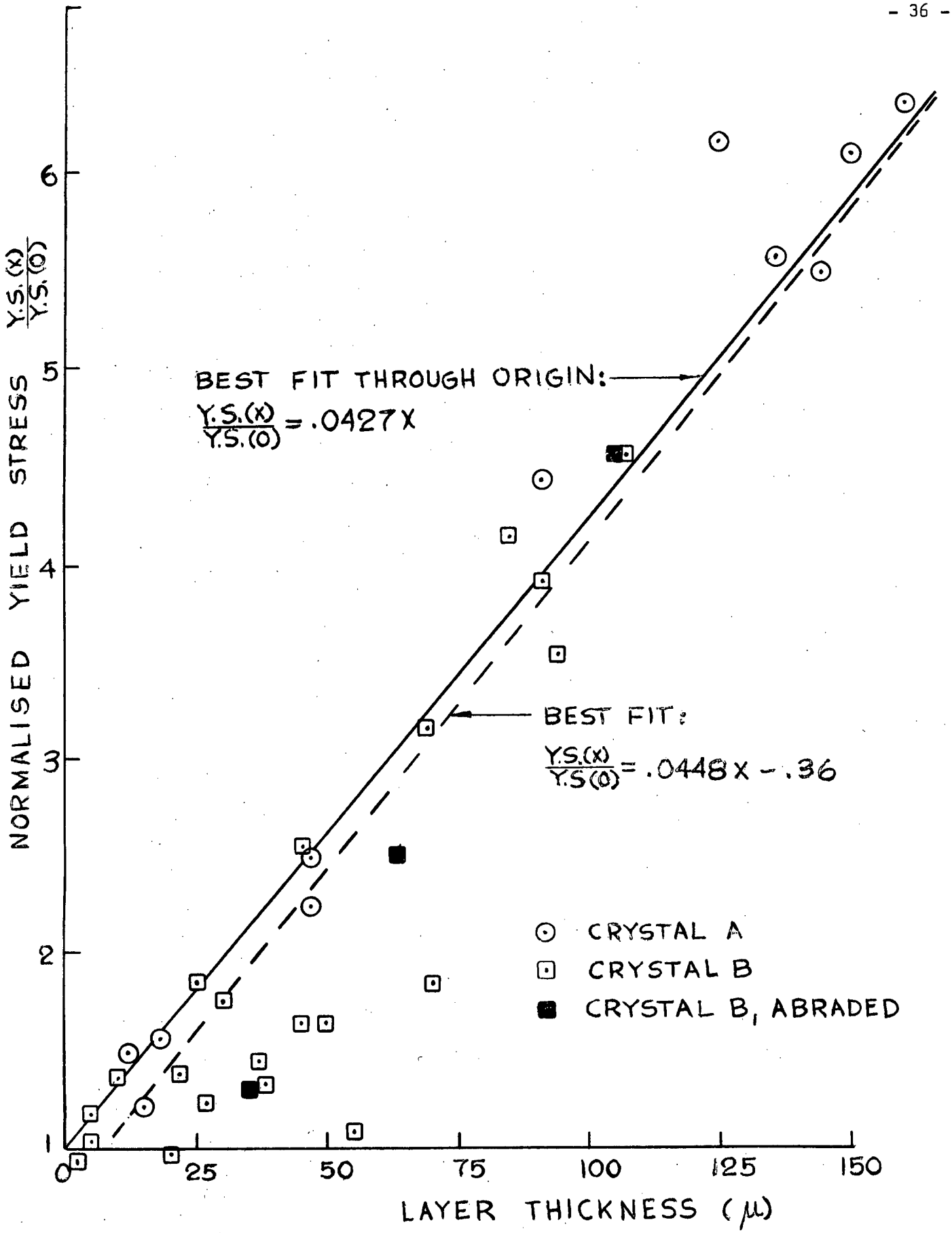

Fig. 26. Variation of yield stress with layer thickness

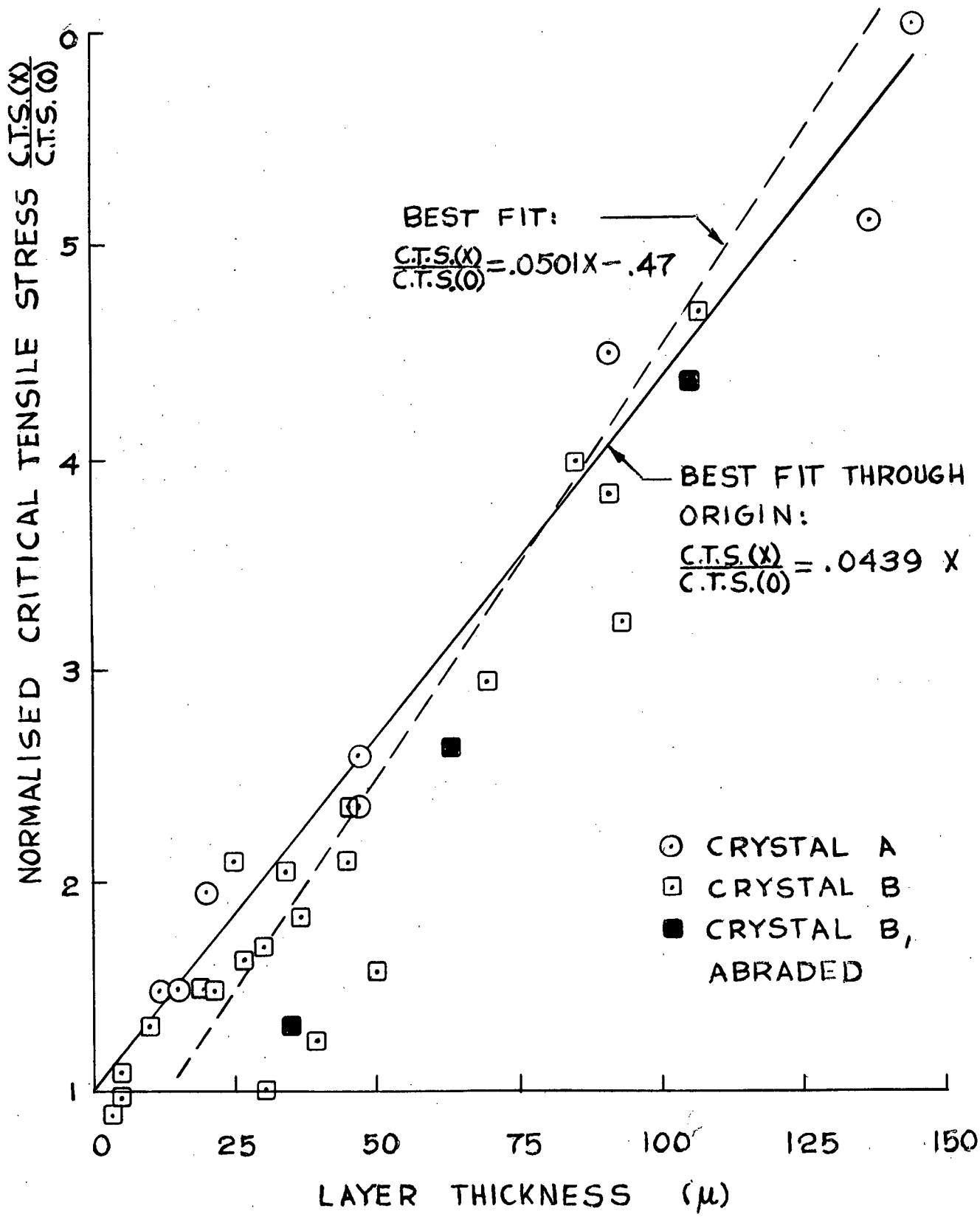

Fig. 27. Variation of critical tensile stress with layer thickness.

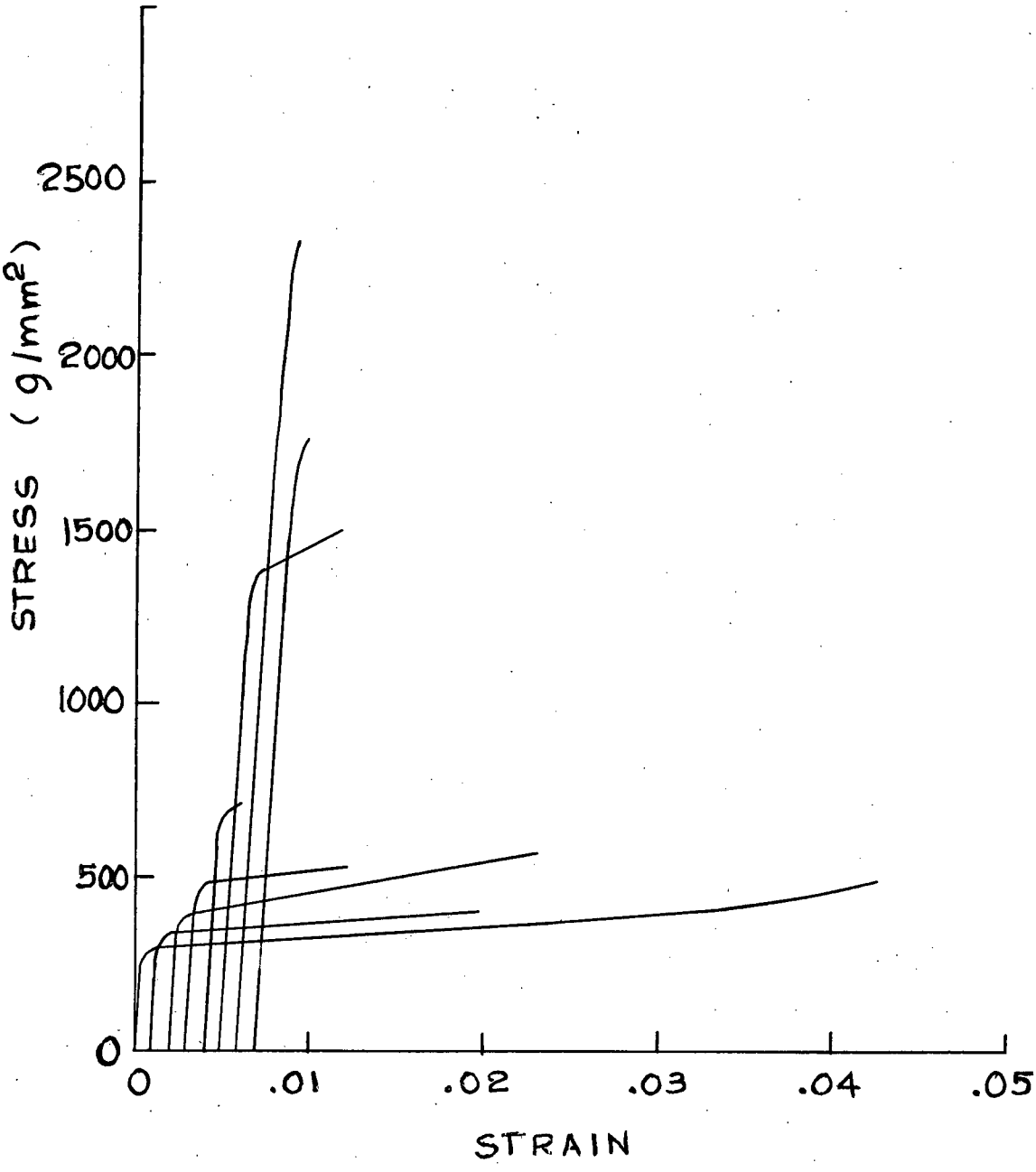

Fig. 28. Typical stress-strain curves for coated crystals.

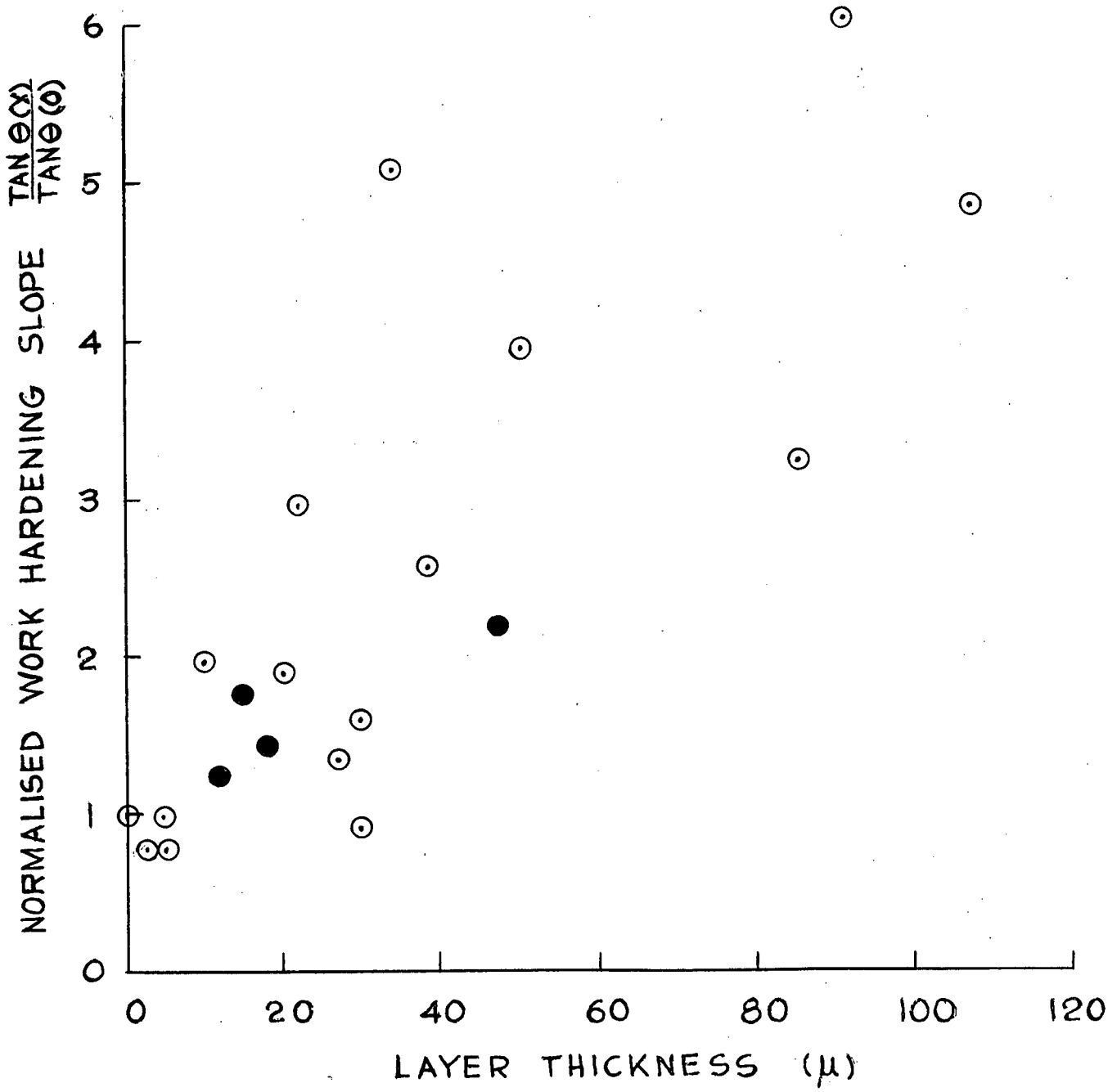

Fig. 29. Variation of initial work-hardening slope with layer thickness.

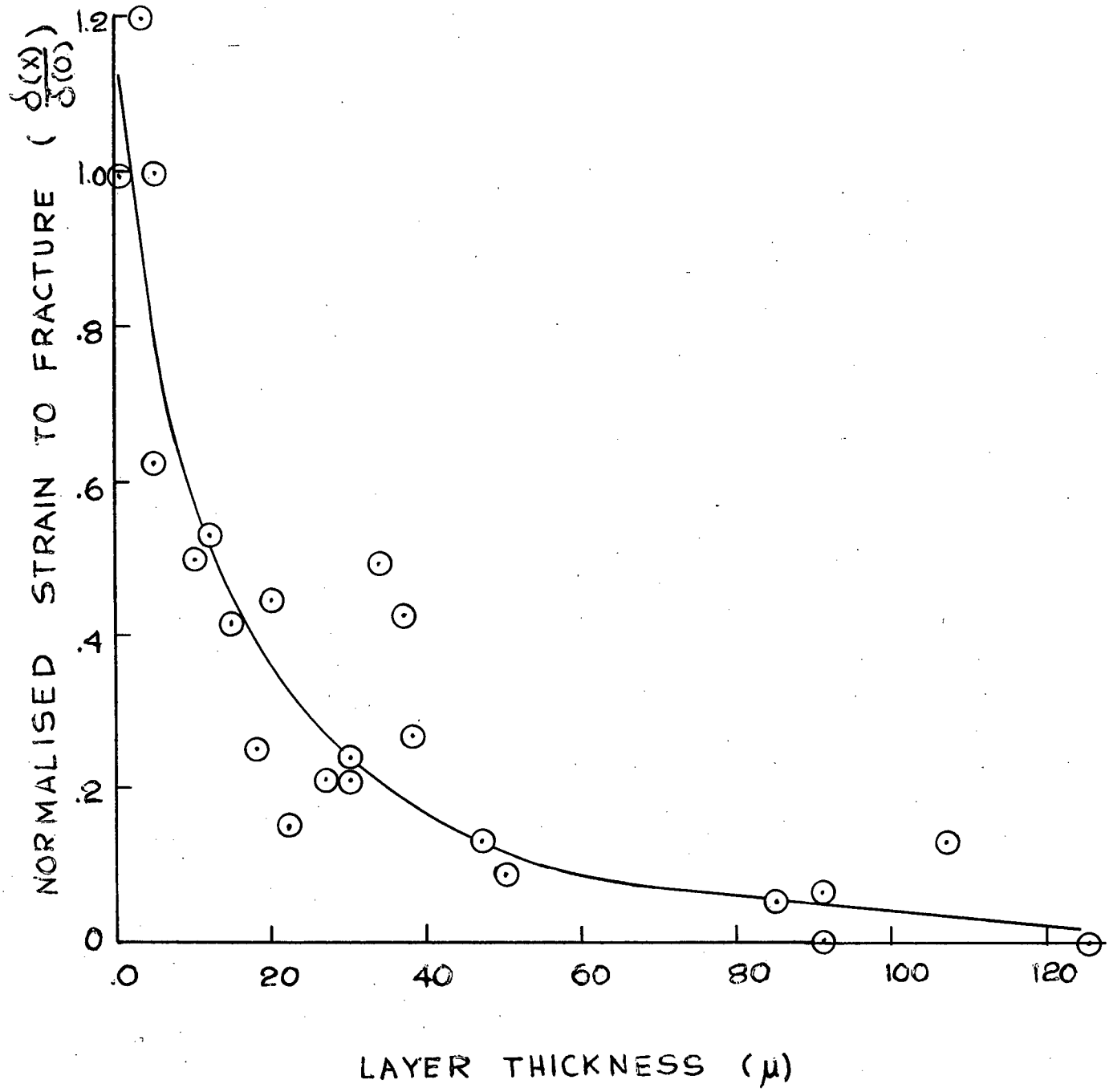

Fig. 30. Variation of the strain to fracture with layer thickness.

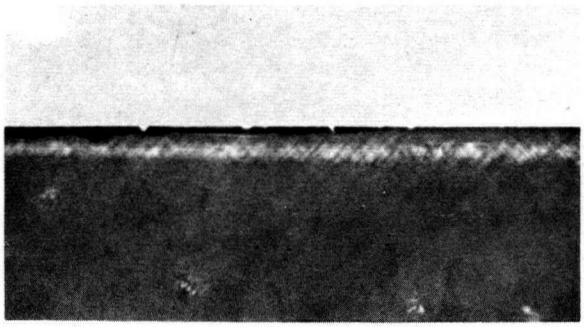

Fig. 31. Birefringence at the diffused layer -- crystal interior interface. 75X

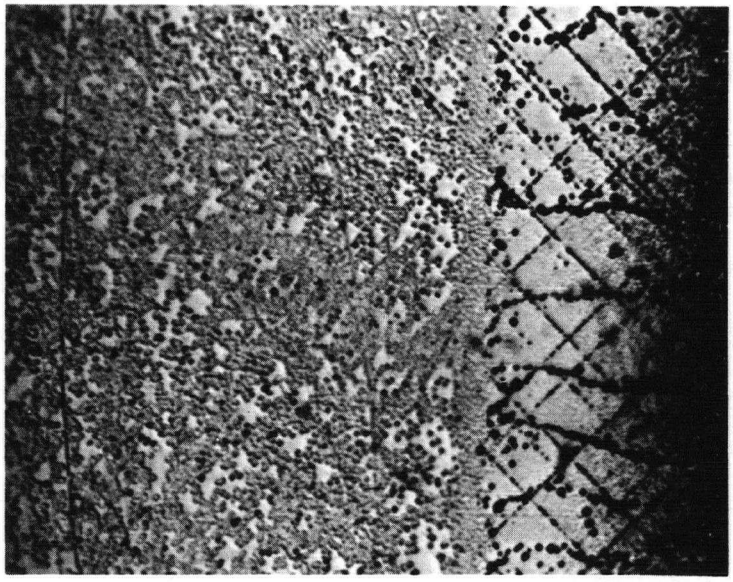

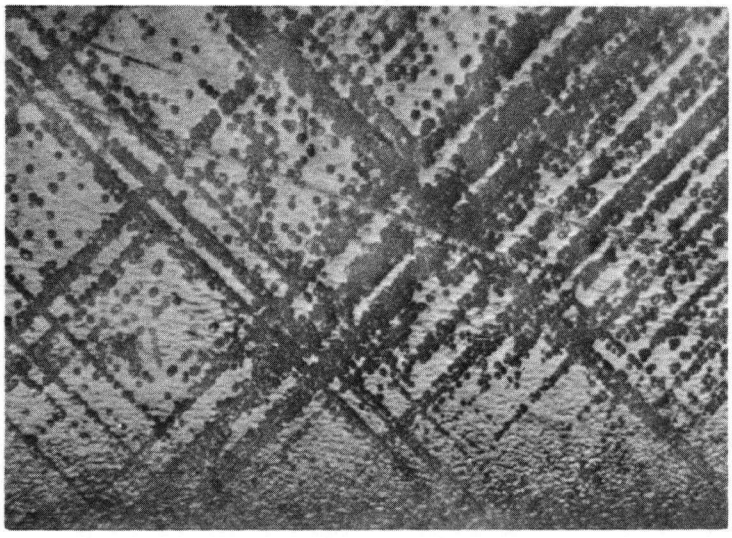

Fig. 32. Photo-micrographs of diffused layers. 280X

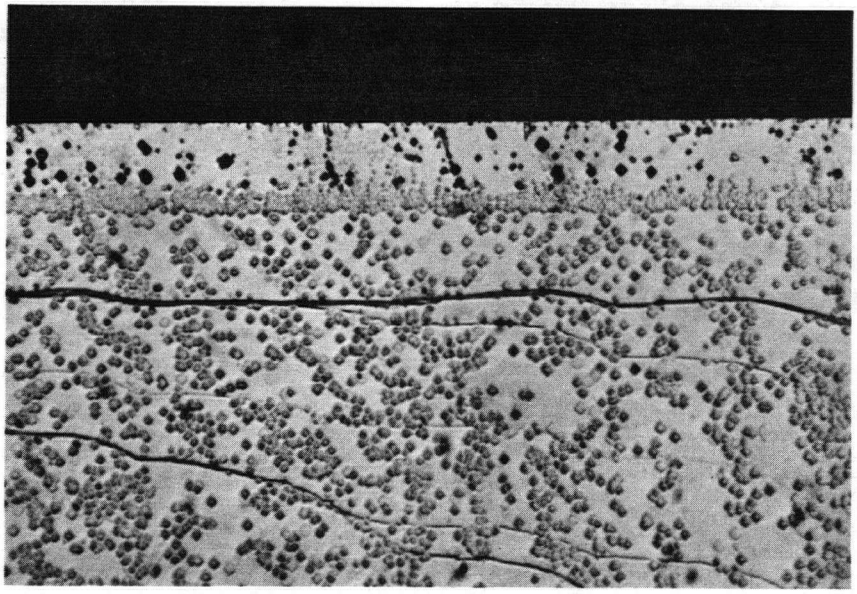

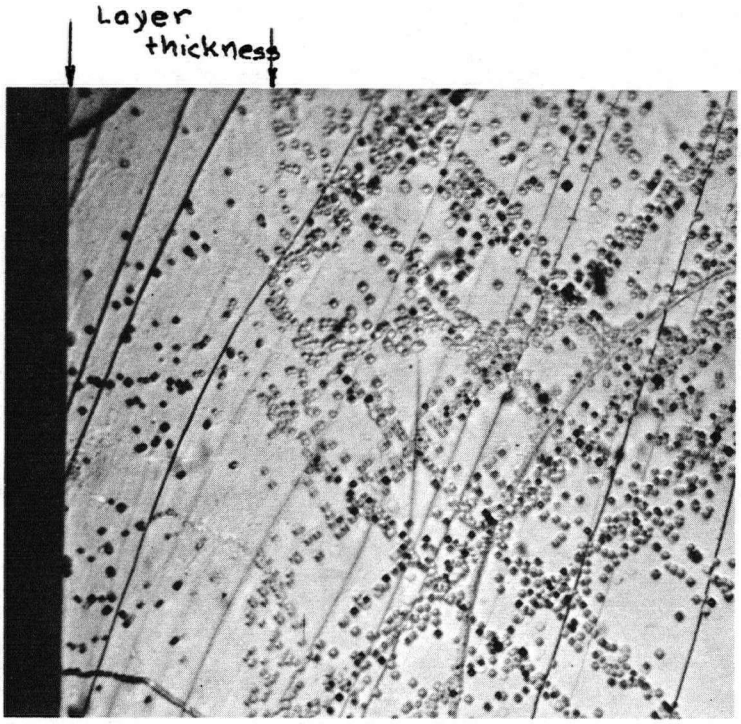

Fig. 33. Photo-micrographs of diffused layers. 280 X

The work-hardening slopes of those specimens which exhibited enough plasticity for the slopes to be measurable are plotted against layer thickness in Fig. 29.

Coatings thicker than 30 μ embrittled the specimens severely as shown in Fig. 30.

The results pertaining to coated crystals are tabulated in Appendix V.

(v) Metallographic observations on coated and deformed crystals.

(a) Observations of birefringence.

Slip bands were observed in every specimen which had been tested, even in those which had failed in an essentially brittle manner. Fig. 31 shows typical photographs obtained under crossed nicols. The interfaces between the diffused layers and the specimen interiors exhibited marked birefringence, as is shown in Fig. 31.

(b) Etch-pit observations.

The dislocation density in the crystal interior was measured on selected specimens which had been strained and sectioned. Three general observations were:

(1) The density of dislocations varied by a factor of approximately two in any one specimen.

(2) The mean dislocation density was approximately 5×10^6 dislocations/$_{cm^2}$ as determined by area counts.

(3) The dislocation density was always low in the diffused layers. In thick diffused layers, the density was equal to that of unstrained crystals ($5 \times 10^4/_{cm^2}$)

The distribution of etch-pits was, in the majority of cases, uniform -- little evidence of distinct slip bands was found. Typical photo-micrographs are shown in Fig. 32 and Fig. 33.

A band of high dislocation density, approximately 10 μ wide, was always observed at the diffused layer -- pure crystal interface. Recognizable

dislocation pile-ups were only rarely observed. An example of a pile-up is shown in Fig. 34.

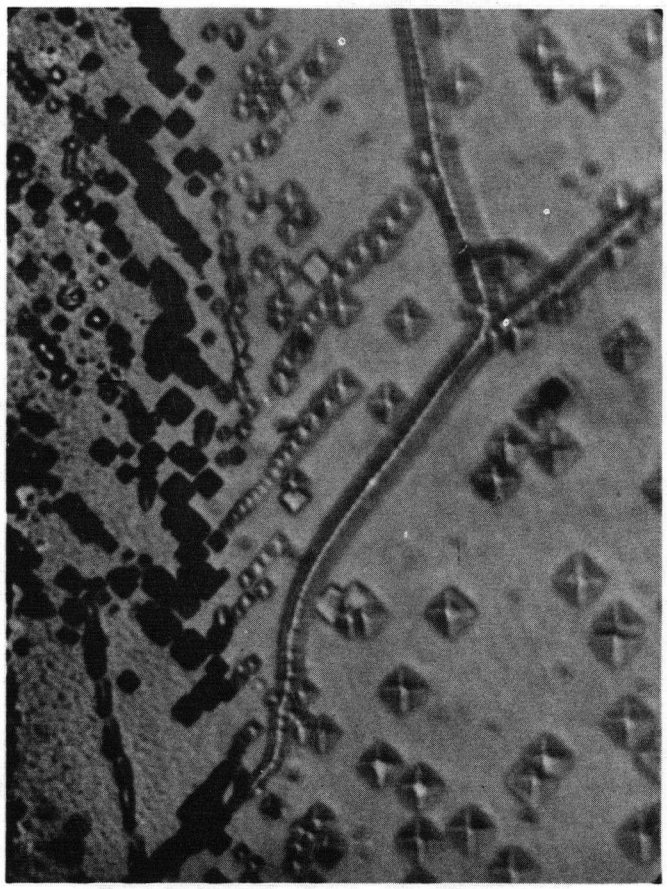

Fig. 34. A short pile-up of dislocations against the diffused layer. 420X

DISCUSSION

(I) Uncoated crystals.

(1) Tensile tests

It has been established by W.G. Johnston that the mechanical properties of LiF are highly sensitive to impurity content, and that the impurity content of crystals obtained from The Harshaw Chemical Co. is variable. A change in the concentration of magnesium from 3 ppm. to 75 ppm. can change the critical resolved shear stress of LiF (at room temperature) from 170 g/mm^2 to a value from 300 g/mm^2 to 1750 g/mm^2, depending on heat treatment[11]. The strength properties of impure LiF are strongly dependent on the cooling rate from temperatures greater than 200°C, increasing rapidly with cooling rate. The strength properties of relatively pure LiF are independent of cooling rate for rates less than 10^3 °C min^{-1}.

A comparison of the critical resolved shear stresses of crystals A and B with those used in the investigations of Johnston[11] suggests that the magnesium contents of both A and B were approximately 10 ppm.

A theory of the rapid hardening induced in LiF by trace amounts of magnesium has very recently been proposed by Fleischer[23].

The causes of the irreproducibility (observed by all current investigators) in:

(1) The appearance of the initial region of the stress-strain curve of LiF, and

(2) The amount of strain to fracture are well understood.

Pure LiF tested at room temperature under very carefully controlled conditions has been shown to exhibit a large (30%) yield drop[10]. However, the specimen alignment must be controlled by rather elaborate procedures in order to observe a reproducible yield drop. Such procedures were not applied in the present investigation. It should be noted, however, that a moderate degree of non-axiality of loading has (empirically) been shown not to change the critical re-

solved shear stress by more than 8%.[1,9,21]

It has been shown that cracks can be generated during plastic flow in ionic crystals by the interaction of dislocations moving on intersecting slip planes.[24,25] In LiF, cracks lying in {100} planes have been found to nucleate at the intersection of pairs of conjugate {110} slip planes.[24] It is therefore apparent that the strain to fracture in LiF crystals is a sensitive function of the slip distribution. The slip distribution, in turn, depends sensitively on the geometrical distribution of dislocation sources operating in the very early (non-elastic) portion of the stress-strain curve, since it has been shown that a whole slip band can arise from one initial mobile dislocation half-loop by multiplication processes. Mobile surface half-loops are inevitably introduced during handling. (It has recently been seriously suggested that stable dislocation half-loops can be introduced into relatively pure LiF by atmospheric dust particles impinging on the crystals.[15]) Hence, it is not unreasonable to expect that the strain to fracture will vary greatly in LiF unless very stringent control indeed is exercised during handling and testing.

The relationship between the amount of ductility and the distribution of slip observed in this investigation is consistent with current theories of crack nucleation in ionic solids.

(ii) Strain rate change tests

It is known[7] that the average velocity of an individual dislocation in strained LiF can be accurately expressed in the form:

$$v(\rho,\sigma) = f(\rho)\left(\frac{\sigma}{\sigma_0}\right)^m \qquad (1)$$

where ρ = dislocation density

σ = applied stress

m = a constant, $16 \leq m \leq 25$, independent of ρ and σ

For any plastic deformation process, the following relation holds:

$$\dot{\epsilon} = c_s b \rho_a v \qquad (2)$$

where $\dot{\epsilon}$ = the tensile strain rate of the specimen

C_s = an appropriate geometrical factor

b = burger's vector

ρ_a = the area density of moving dislocations

Consider an idealized strain rate change test (one in which the change of crosshead speed is instantaneous) resulting in an observed load-elongation curve similar to the one shown in Fig. 35.

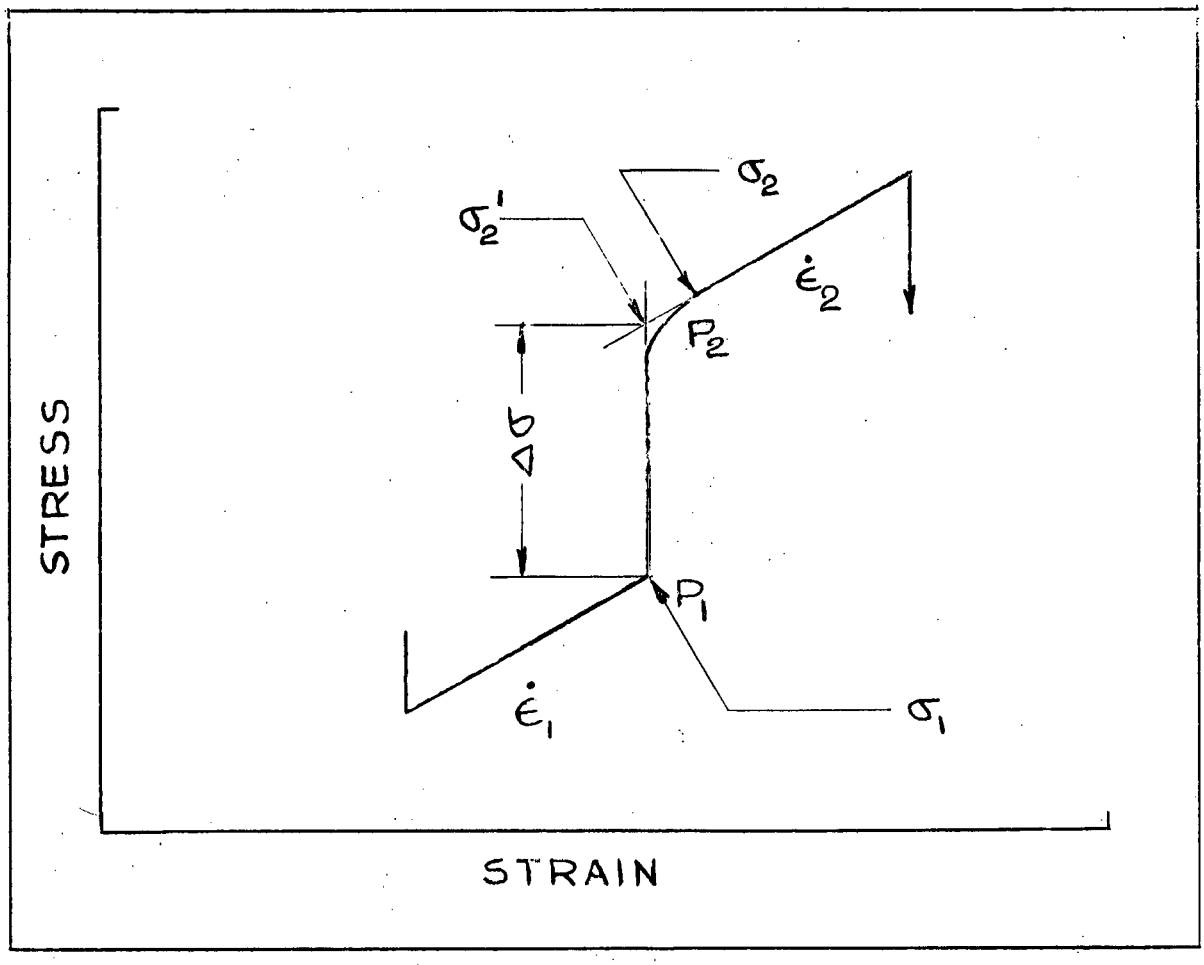

Fig. 35. Parameters observed in an idealized strain rate change test.

Let the parameters v and ρ take the values (v_1,ρ_1) and (v_2,ρ_2) at the points P_1 and P_2. Let the conventionally defined flow stresses at P_1 and P_2 be σ_1 and σ_2. Then:

$$\frac{\dot{\epsilon}_2}{\dot{\epsilon}_1} = \frac{\rho_2 v_2}{\rho_1 v_1} = \gamma > 1 \qquad (3)$$

where γ = a constant independent of stress

If it is now assumed that:

(1) $\rho_1 = \rho_2$

(2) $\sigma_2' = \sigma_2$ (i.e. The flow stress at P_2 is sufficiently well represented by the usual convention.)

then:

$$\gamma^{\frac{1}{m}} = \left(\frac{\sigma_2}{\sigma_1}\right) = \frac{\Delta\sigma}{\sigma_1} + 1 \qquad (4)$$

$$\text{i.e. } \frac{\Delta\sigma}{\sigma_1} = \gamma^{\frac{1}{m}} - 1 > 0 \qquad (5)$$

That is, a Cottrell-Stokes law follows from the premises:

(1) $v(\rho,\sigma) = f(\rho)g(\sigma)$

(2) $g(\sigma) = O(\sigma^m)$

(3) $\rho_1 = \rho_2$

A Cottrell-Stokes law is not observed in LiF. (1) and (2) are experimental facts. It follows that equation (4) is in error and that the correct form of (5) is:

$$\frac{\Delta\sigma}{\sigma_1} = \gamma^{\frac{1}{m}}\left[\frac{\rho_2 f(\rho_2)}{\rho_1 f(\rho_1)}\right]^{\frac{1}{m}} - 1 \qquad (6)$$

That is, the observed $\Delta\sigma$ is not even approximately attributable to the change in the mean dislocation velocity. Instead, the magnitude of $\Delta\sigma$ is governed by a combination of a change in the number of mobile dislocations (caused by multiplication processes, perhaps according to the theory of Wiedersich[26].) and a change in the mean dislocation velocity. The assignation of a single activation energy to the process resulting in the observed $\Delta\sigma$ is therefore meaningless.

Independent evidence of the validity of this conclusion exists. From equation (2) it follows that:

$$\frac{d(\log\dot{\epsilon})}{d(\log\sigma)} = \frac{d(\log v)}{d(\log\sigma)} + \frac{d(\log\rho)}{d(\log\sigma)} \qquad (7)$$

Direct measurements of $\frac{d(\log\dot{\epsilon})}{d(\log\sigma)}$ and $\frac{d(\log v)}{d(\log\sigma)}$ have been performed on LiF[1,27], silicon iron[28,29], and Ge[30]. For all of these materials it has been shown that:

$$\frac{d(\log v)}{d(\log\sigma)} \cong \frac{d(\log\rho)}{d(\log\sigma)} \qquad (8)$$

That is, a change in strain rate is accompanied by a change in both the number and the mean velocity of mobile dislocations. It should be noted that the increase in the number of mobile dislocations is not physically unreasonable in that it does not imply extensive motion of dislocations in a perfectly elastic region of the stress-strain curve. The implication is simply that for a given increase in plastic strain, the mean number of dislocations moving is a sensitive function of the mean stress prevailing during the strain increase. Studies of individual dislocation multiplication events in unstrained LiF[8] have shown that this is indeed so.*

When the crosshead of a testing machine is suddenly stopped, an instability occurs in the dynamic equilibrium between the time rates of change of dislocation production, debris production, and dislocation velocity which is established during a tensile test. It does not, however, immediately follow that any one of these quantities becomes zero instantaneously, or even that they approach zero at approximately equal rates. It is premature to speculate on the details of the events occurring during strain rate changes in view of the fact that the

---

*It has been shown that:

$$\frac{dn}{dt} = A e^{-\frac{B}{\sigma}}$$

where n = number of loops emitted in 1 second when a dislocation moves.

σ = applied stress

The measurements were conducted in the domain 1.6×10^8 dynes/$_{cm^2} \leq \sigma \leq 5 \times 10^8$ dynes/$_{cm^2}$; the corresponding range of $\frac{dn}{dt}$ is:

$$10^{-3} \text{ loops/sec} \leq \frac{dn}{dt} \leq 10^{9} \text{ loops/sec}$$

current theories of work-hardening in LiF are not yet fully quantitative. It should be noted, however, that:

(1) The irreversibility of the first kind is not caused by creep. For 100:1 strain rate changes, the amount of extension of the specimen required to account for the observed strengthening by normal work-hardening is approximately $\frac{1}{2}$ mm. The amount of (elastic) extension required to completely unload the specimen is calculated to be 10^{-2} mm.

(2) Known strain-aging processes are not involved in the irreversibilities observed. A time of the order of 1 hour at a temperature of 120°C is required to lock dislocations in relatively impure LiF[10]. Also, the fact that negligible strengthening of the specimens occurs if they are rapidly unloaded and held in the unloaded condition for times comparable to the time required to effect the strain rate changes excludes the possibility of strain-aging processes occurring.

The fact remains, however, that LiF does harden on unloading and that the amount of hardening increases with the stress prevailing during straining. This suggests that, during unloading, the debris production rate decreases less rapidly with stress than does the dislocation velocity.

Haasen has recently reported similar "irreversible effects" while investigating strain rate change phenomena in NaCl.[31] The early portion of the $\Delta\sigma$ versus σ curve in silicon iron also exhibits irreversibilities.[29]

(iii) Polishing effects

Only very general conclusions may be drawn from the essentially exploratory investigation of the effect of removing surface layers during tension testing:

(1) The equilibrium dislocation distribution in strained LiF is not the same throughout the whole crystal.

(2) The distribution of dislocations in LiF is not the same in all stages of the stress strain curve.

(3) The surface is not a preferred site of work-hardening in LiF.

(4) The effects of surface removal are not large unless relatively thick layers (more than 20 μ) are removed.

Conclusion (3) is in agreement with Mendelson's work on NaCl,[32] but is in disagreement with the results of Suzuki for KCl.[33] (The adequacy of Suzuki's experimental procedure has recently been questioned.[32])

II Coated crystals

(i) The properties of the diffused layers

Two obvious inconsistencies in the properties of the magnesium-rich layers are:

(1) The micro-hardness profiles suggest that solutions of the diffusion equation relating to diffusion from an instantaneous plane source of strength Q are appropriate.

(viz. $C(x,t) = \frac{Q}{\alpha t} e^{-\frac{x^2}{Dt}}$)

(2) The observation that magnesium was present in excess suggest that solutions of the form

$$C(x,t) = C_0(T) \operatorname{erfc} \frac{x}{\sqrt{Dt}}$$

are relevant.

In view of these inconsistencies and since no systematic temperature or time dependence of the layer thickness was established, it is apparent that some essentially uncontrolled variable governed the diffusion kinetics during this investigation. Accidental surface contamination and a variable residual gas composition in the diffusion vials may conceivably have influenced the diffusion kinetics markedly, although the remarkable uniformity of the character of the diffused layer on any one crystal suggests that surface contamination was not an important factor. The correlations attempted in this investigation are, in any case, based on the independently measured properties of the diffused layers.

The quantitative correlation of hardness measurements with tensile properties is difficult. For any given material and within restricted ranges of hardness, the existence of a general correlation of the form:

$$\frac{U.T.S.(1)}{U.T.S.(2)} = \frac{H(1)}{H(2)} \qquad (9)$$

has been established.[34]

It has proved possible to establish an analogous empirical correlation between Knoop hardness and the flow stress of LiF at 0.06% strain (as measured in bending) from the data of Nadeau.[35]

It is:

$$\frac{\sigma_{F(1)}}{\sigma_{F(2)}} = 2.1 \frac{K.H.(1)}{K.H.(2)} \qquad (10)$$

Unfortunately, this correlation is established from data relating to LiF crystals ten times harder than those used in the present investigation and must therefore be regarded as tentative.

If an extrapolation of (10) is accepted as valid, the yield stress of the isolated diffused layers was approximately three times that of the pure LiF crystals. Even in view of the uncertainties implicit in the application of (10) to the present case, it seems safe to conclude that the yield stress of the diffused layers was at most six times greater than that of the pure LiF.

The X-ray investigation of the nature of the diffused layers shows that:

(1) The amount of second phase (MgF_2) present, if any, was too small to be detected by the Debye-Sherrer technique.

(2) The lattice parameter of the magnesium-rich LiF was identical with that of pure LiF to within 0.002Å.

(3) The diffused surface layers were single crystals, coherent with the substrate.

(2) Tension tests

Assume that no interaction occurs between the crystal interior and the diffused layer during a tension test. Define:

σ_0 = yield stress of the pure crystal
σ = yield stress of the diffused layer
σ' = yield stress of the combination

("yield stress" is to be interpreted as the stress necessary to establish a given small dislocation velocity)

It follows immediately that:

$$\frac{\sigma}{\sigma_0} = \frac{\frac{\sigma'}{\sigma_0} - \left(1 - \frac{4x}{d}\right)}{4\frac{x}{d}} \qquad (11)$$

where x = thickness of the diffused layer
d = the side of the cross section of the specimen

From the data in Fig. 26,

$$\frac{\sigma}{\sigma_0} = 22 \quad (\text{at } x = 100\mu) \tag{12}$$

A value of 5500 $g/_{mm}2$ for the yield stress of magnesium doped LiF cannot be rejected a priori, in view of the known strong hardening effect of magnesium on LiF. Several reasons are, however, apparent why such a large value for the yield stress of the diffused layers is not credible:

(1) The micro-hardness measurements suggest that $\frac{\sigma}{\sigma_0} \simeq 6$.

(2) When a diffusion run was terminated, the furnace was cooled at approximately $\frac{1}{2}^{o}C$ per minute. It is known that in order to obtain great strengthening, magnesium-containing LiF must be cooled at rates of the order of $10^{-2}{}^{o}C\ min^{-1}$.

(3) LiF containing 0.5 mol. % magnesium has a yield stress of approximately 6000 $g/_{mm}2$ when slow cooled[34]. However, large characteristic MgF_2 precipitate particles are seen in such highly alloyed LiF. No evidence of a precipitate was found in the diffused layers during the present investigation.

(4) The maximum solubility of magnesium in LiF varied from 0.03 mol. % to 0.40 mol. % at the temperatures prevailing during the diffusion runs. In view of the fact that little variation in the etching behaviour of the layers on different crystals was observed, it is apparent that the solubility limit was not attained. This establishes an upper bound of approximately 300 ppm on the concentration of magnesium in the layers. Such a value is also consistent with the micro-hardness measurements.

It can therefore be concluded that a large degree of interaction exists between the diffused layers and the crystal interior during tension tests.

Of the four fundamental mechanisms proposed by Machlin, three are, in principle, applicable to the present system. The "force-field" effect and the associated edge dislocation pile-ups proposed by Head[17] may be excluded since Nadeau has shown that the Young's modulus of LiF is not changed greatly by

magnesium alloying.[35]

The linear dependence of the yield stress on the layer thickness up to very thick layers suggests that either:

(1) Fisher type surface sources do not exist in LiF, or

(2) The yield stress is not the stress required to activate surface sources (or both).

The metallographic evidence shows that, in specimens possessing thick diffused layers, dislocations were nucleated and multiplied much more readily in the crystal interior than in the diffused layers. The evidence was less clear in the case of thin layers since the specimens were strained a large amount before being sectioned. Even in these cases, however, less dislocation activity had apparently occurred in the layers than in the crystal interior. If it is assumed that the mechanical properties of thick and thin layers were nearly identical, it follows that at the beginning of plastic flow, dislocations were in all cases generated more easily in the crystal interior than in the layers. Since the yield stress of a specimen with a 20 μ layer was only 50% greater than that of pure crystal, it follows that the yield stress was not determined by surface source operation. Instead, dislocations were nucleated in the crystal interior at stresses below the macroscopically determined yield stress, and multiplied profusely before emerging from the crystals.

The processes whereby dislocations are nucleated in LiF are not fully understood at present, as it has been shown that the grown-in Frank network does <u>not</u> act as a source of dislocations, at least in crystals of presently available purity.[1-10] It has also been shown that dislocations do not arise homogeneously in perfect regions of LiF crystals even at stresses as high as $\frac{G}{85}$.[6] The present work indicates that dislocations either do not arise preferentially near the crystal surface, or the yield stress is not determined by source operation, or both.

Evidence has been presented that edge dislocations pile up at the interface

between the diffused layer and the crystal interior. The strengthening caused by the layers is probably associated with this pile-up phenomenon. However, it is impossible, at the present state of knowledge, to develop a quantitative theory of the strengthening.

It should be noted that the mere existence of short pile-ups cannot greatly change the increment of plastic strain occurring at a given mean stress, since:

$$\epsilon = b\rho\frac{X}{A} \qquad (13)$$

where X = mean slip distance of the moving dislocations

and hence:

$$\frac{\delta\epsilon}{\epsilon} = \frac{\delta X}{X} \simeq \frac{10\mu}{2.5\times10^{3}\mu} = 4\times10^{-3} \qquad (14)$$

That is, it is not possible to attribute the increased rate of work-hardening or the increased yield stress merely to the small changes in the mean slip distance of glide dislocations which a short pile-up causes.

The multiplication rate of screw dislocations may be affected by back stresses from the piled-up groups, but in view of the fact that the mechanism of dislocation multiplication in LiF is not yet fully understood,[26,36,37,38] speculation on this point is premature.

The decrease in ductility caused by the presence of a diffused layer is undoubtedly associated with the piling up of edge dislocations against the layer. Crack nucleation by the mechanism proposed by Stroh[39] or by a variation thereof[40] probably occurs at the interface, and the cracks grow according to the mechanism proposed by Griffiths.[41]

The results of the present investigation cannot be compared in detail with the work of Westwood for the following reasons:

(1) The alloyed layers were prepared by different techniques in the two investigations.

(2) The greater part of Westwood's work was concerned with the locking of artificially introduced surface sources.

There are certain points of conflict, however, between the results of Westwood and those of the present author:

(1) Westwood observed that the initial rate of work-hardening increased rather less rapidly with layer thickness than the trend established in this investigation indicates.

(2) Largely as a consequence of (1), Westwood observed that the ultimate tensile stress of the coated crystals was often reduced to half of that of uncoated crystals. In the present investigation, the ultimate tensile strength of coated crystals was always larger than the average value for uncoated crystals.

(3) Regarding (apparently) one experiment on a polished and coated crystal [3] Westwood states ".... the reaction treatment had very little effect on its yield stress (an increase of 3%) and caused only a small increase in the critical resolved shear stress (13%)". Unfortunately, no data on the coating thickness are provided. (Generally, Westwood differentiates only between thin ($\nsim 10\,\mu$) and thick ($\approx 25\,\mu$ and $\ngtr 50\,\mu$) coatings.) The present investigation shows that it is possible to increase both the yield stress and the critical resolved shear stress of polished crystals by 250% by producing 50 μ thick alloyed layers.

It seems to be implied throughout Westwood's communication that a magnesium-alloyed layer has relatively little effect on the strength properties of polished LiF crystals. The hardening observed in as-cleaved and coated crystals is attributed to the locking of artificially introduced surface dislocation sources by magnesium. However, the present investigation shows that it is possible to strengthen <u>polished</u> LiF crystals appreciably by producing a magnesium rich surface layer. Surface source locking effects seem to contribute little to the strengthening.

SUMMARY AND CONCLUSIONS

(1) It is possible to perform adequate tensile tests on LiF single crystals while taking only moderate precautions.

(2) The change of flow stress observed during strain rate change tests is not determined solely by a change in the mean velocity of previously mobile dislocations. The number of mobile dislocations apparently changes greatly during both increases and decreases of strain rate. Hence, an *a priori* application of the current rate theory formalism to work-hardening processes constitutes a serious over-simplification.

(3) During stress relaxation, dislocation activity prevails in LiF. The hardening caused by this activity increases with the level of stress from which relaxation occurs. This implies that macroscopic plastic deformation is not prerequisite to strain hardening.

(4) Preliminary evidence exists that the distribution of dislocations in a rather thick ($\simeq 80\,\mu$) surface layer is not identical with that existing in the interior of strained LiF crystals. The difference in distribution appears to be associated with macroscopic effects which are more complex than a preferential surface layer hardening phenomenon.

(6) The yield stress and/or the critical resolved shear stress of chemically polished LiF are not the stresses required to activate dislocation sources existing near the crystal surface.

SUGGESTIONS FOR FURTHER WORK

The present work could be extended in many directions:

(1) The properties of LiF at high strain rates (10^{-2} sec^{-1} to 1 sec^{-1}) appear to be interesting. Adequate instrumentation for their study should prove easy to develop.

(2) A careful photo-elastic study, utilizing high speed cinematography, should prove fruitful, contingent on the development of unambiguous quantitative dislocation models of the birefringence effects.

(3) The present work on surface coatings might well be repeated, using more refined techniques of coating preparation.

(4) The effects of removing surface layers during deformation should be investigated more thoroughly.

(5) A study of the temperature variation of the mechanical properties of LiF would probably <u>not</u> prove illuminating at the present time.

REFERENCES

1. J.J. Gilman and W.G. Johnston, Dislocations and Mechanical Properties of Crystals, J.C. Fisher ed., Wiley, N.Y. 116, (1957)

2. J.J. Gilman, Progress in Ceramic Science vol. I, J.E. Burke ed., Pergamon Press N.Y. (1960)

3. J.J. Gilman and W.G. Johnston, Solid State Physics 13, D. Turnbull ed. (1962)

4. J.J. Gilman and W.G. Johnston, Jour. App. Phys. 29, 877 (1958)

5. J.J. Gilman and W.G. Johnston, Jour. App. Phys. 30, 129 (1959)

6. J.J. Gilman, Jour. App. Phys. 30, 1584 (1959

7. W.G. Johnston and J.J. Gilman, Jour. App. Phys. 31, 632 (1960)

8. J.J. Gilman and W.G. Johnston, Jour. App. Phys. 31, 687 (1960)

9. J.J. Gilman, Jour. App. Phys. 33, 2703 (1962)

10. W.G. Johnston, Jour. App. Phys. 33, 2716 (1962)

11. W.G. Johnston, Jour. App. Phys. 33, 2050 (1962)

12. J.J. Gilman, Jour. App. Phys. 4, 601 (1958)

13. J.J. Gilman, Acta Met. 7, 123, (1961)

14. I.R. Kramer and L.J. Demer, Prog. in Metal Phys. 9, (1960)

15. E.S. Machlin, Strengthening Mechanisms in Solids, A.S.M. Seminar, 375 (1962)

16. A.C.R. Westwood, Phil. Mag. 6, 542 (1961)

17. A.K. Head, Proc. Phil. Mag. 44, 92 (1953)

18. E.D. Shchukin, Proc. Acad. Sci. U.S.S.R. 118, 1105 (1958)

19. F.R.N. Nabarro, Advances in Physics 1, 269 (1952)

20. J.J. Gilman, Phil. Mag. 6, 159 (1961)

21. A.R.C. Westwood, Phil. Mag. 5, 981 (1960)

22. R.F. Snowball, Unpublished M.A.Sc. thesis, The University of British Columbia (1960)

23. R.L. Fleisher, Jour. App. Phys. 33, 3504 (1962)

24. W.G. Johnston, Phil. Mag. 5, 407 (1960)

REFERENCES CONTINUED

25. R.J. Stokes, T.L. Johnston, and C.H. Li, Strengthening Mechanisms in Solids, A.S.M. Seminar, 341 (1962)

26. H. Wiedersich, Jour. App. Phys. 33, 854 (1962)

27. W.L. Phillips, Trans. A.I.M.E. 218, 939 (1960)

28. D.F. Stein and J.R. Low, Jour. App. Phys. 31, 362 (1960)

29. R.W. Guard, Acta Met. 9, 163 (1961)

30. A.R. Chaudhuri, J.R. Patel, and L.G. Rubin, Jour. App. Phys. 33, 2737 (1962)

31. P. Haasen, Jour. App. Phys. 29, 718 (1958)

32. S. Mendelson, Jour. App. Phys. 33, 2182 (1962)

33. T. Suzuki, Dislocations and Mechanical Properties of Crystals, J.C. Fisher ed. Wiley, N.Y. 215 (1957)

34. Data by Wilson Mechanical Instrument Division, American Chain & Cable Co., Inc.

35. F. Nadeau, Unpublished Ph.D. Thesis, University of California, (1959)

36. F. Tetelman, Acta Met. 10, 1021 (1962)

37. J.C.M. Li and C.D. Needham, Jour. App. Phys. 31, 1318 (1960)

38. A.S. Argon, Acta Met. 10, 574 (1962)

39. A.N. Stroh, Phil. Mag. 46, 986 (1955)

40. A.H. Cottrell, Trans. A.I.M.E. 212, 192 (1958)

41. A.A. Griffiths, Trans. Roy. Soc. (London) A 221, 180 (1921)

APPENDIX I

ESTIMATES OF ERROR

(1) Uncertainties in measurements

It is apparent that:

$$\frac{\delta S}{S} = \frac{\delta F}{F} + \frac{\delta A}{A} = \frac{\delta F}{F} + 2\frac{\delta X}{X}$$

where A = stress
F = force
A = specimen cross-section
X = edge of cross-section

i.e. $\frac{\delta P}{P} = .01 + (2)\frac{(.005)}{2.5} = .015$

(2) Uncertainties in parameter measurements from the chart.

(a) The yield point could be determined to $\pm$ .10 lbs. in 4 lbs.

$$\therefore \delta(\text{Y.P.}) = \frac{.10}{4} = .025$$

(b) The critical tensile stress could be determined to 0.01 lbs. in 4 lbs.

$$\therefore \delta(\text{C.T.S.}) = \frac{.01}{4} = .003$$

Therefore, the total uncertainties in the absolute values of the strength parameters due to errors of measurement are:

$$\delta_t(\text{Y.P.}) \not> 5\%$$
$$\delta_t(\text{C.T.S.}) \not> 2\%$$

(3) The effect of non-axiality.

On the basis of elasticity theory, the distribution of stress on the specimen cross-section sufficiently far from the grips was linear, such that:

$$\left|\frac{S_{max} - S_{avg}}{S_{avg}}\right| = \frac{6\epsilon}{L}$$

where S_{max} = maximum tensile stress in outer fiber

S_{avg} = average tensile stress

ϵ = distance from centroid of specimen to point of load application

$$\text{i.e.} \quad \left| \frac{S_{max} - S_{avg}}{S_{avg}} \right| \leq \frac{(6)(.2)}{(2.5)(2)} = 0.25$$

This is an upper bound, since the exact value depends on the (unknown) details of the position of the specimen relative to the grips. As deformation proceeds, the stress distribution will become more uniform.

The non-uniformity of stress proved troublesome for specimens possessing thick alloyed layers. However, it was often possible to determine which specimens had been subjected to bending moments by etching the slip bands on a longitudinal section. The results of tests on specimens which showed evidence of having been bent were discarded.

APPENDIX II

Results of Tensile Tests on Uncoated Specimens

Specimen Number	Yield Stress (g/mm^2)	Critical Tensile Stress (g/mm^2)	Ultimate Tensile Stress (g/mm^2)	Total Strain	Work-Hardening Slope ($g/mm^2 \times 10^{-4}$)	Strain Rate ($sec^{-1} \times 10^4$)
A 2	349	387	665	.0433	.640	4.28
A 3	318	388	586	.0251	.780	4.28
A 7	336	419	692	.0471	.581	4.28
A 8	286	428	581	.0156	.972	4.28
A 9	275	351	732	.0508	.747	4.28
A 19	288	338	556	.0437	.510	4.28
A 27	281	386	585	.0359	.566	4.28
B 1	224	285	427	.0359	.395	4.28
B 2	236	282	512	.0522	.441	4.28
B 3	299	318	448	.0284	.456	4.28
B 4	278	316	574	.0532	.485	4.28
B 12	259	295				4.28
B 13	268	281				4.28
B 14	250	296				4.28
B 35	212	289				4.28
B 8	257	307				2.14
B 15	206	231				2.14
B 17	188	244				2.14
B 19	184	244				2.14
B 21	220	254				2.14
B 22	209	235				2.14
B 23	205	243				2.14
B 25	198	263				2.14
B 30	222	279				2.14
B 7	360	421				21.4
B 27	298	329				21.4
B 29	344	445				21.4

Specimen Number	Yield Stress (g/mm^2)	Critical Tensile Stress (g/mm^2)	Ultimate Tensile Stress (g/mm^2)	Total Strain	Work-Hardening Slope ($g/mm^2 \times 10^{-4}$)	Strain Rate ($sec^{-1} \times 10^4$)
B 32		359				21.4
B 33	291	342				21.4
B 18	423	456				214
B 24	501	515				214
B 28		495				214

Note: Only the initial strength properties are listed for the specimens on which Cottrell-Stokes tests were performed.

Average Initial Tensile Properties of
Uncoated Specimens from Crystal A.

Strain Rate (sec^{-1} 10^4)	Yield Stress (g/mm^2)	Critical Tensile Stress (g/mm^2)
2.14	209 ± 7	255 ± 7
4.28	254 ± 18	295 ± 6
21.4	322 ± 8	354 ± 14
214	471 ± 50	490 ± 24

APPENDIX III

Results of Strain Rate Change Tests

Specimen B 8

Strain Rate Cycled by I
($2.14 - 21.4 \times 10^{-4}$ sec^{-1})

σ (g/mm^2)	$\frac{\Delta\sigma}{\sigma_1}$	$\ln(1+\frac{\delta}{L_0})$	σ (g/mm^2)	$\frac{\Delta\sigma}{\sigma_1}$	$\ln(1+\frac{\delta}{L_0})$
310	.122	.0012	653	.088	.0381
328	.143	.0036	671	.076	.0402
349	.185	.0043	680	.083	.0408
378	.114	.0062	699	.072	.0434
384	.116	.0068	707	.082	.0439
408	.109	.0087	728	.068	.0460
409	.150	.0093	738	.077	.0465
433	.117	.0116	755	.068	.0487
437	.133	.0122	764	.076	.0492
449	.120	.0139	781	.068	.0513
455	.120	.0144	789	.077	.0519
456	.119	.0166	811	.063	.0539
476	.114	.0172	823	.069	.0545
487	.099	.0192	843	.063	.0568
494	.114	.0197	850	.074	.0574
507	.099	.0219	869	.064	.0595
515	.106	.0222	879	.071	.0600
530	.089	.0246	900	.063	.0622
536	.100	.0250	907	.073	.0626
554	.082	.0273	927	.062	.0646
559	.098	.0279	939	.070	.0652
577	.079	.0298	956	.067	.0671
582	.095	.0303	971	.064	.0678
595	.087	.0322	992	.060	.0699
604	.090	.0327	1003	.068	.0705
620	.079	.0351	1015	.069	.0725
628	.091	.0356	1029	.067	.0730
643	.076	.0381	1050	.063	.0750

Specimen B 8

σ (g/mm^2)	$\frac{\Delta\sigma}{\sigma_1}$	$\ln(1+\frac{\delta}{L_o})$
1068	.060	.0755
1083	.065	.0783
1094	.066	.0788
1120	.063	.0810
1137	.062	.0816
1158	.058	.0836
1169	.062	.0840
1192	.055	.0860
1206	.061	.0870
1232	.056	.0889
1244	.059	.0895
1256	.061	.0920
1282	.059	.0925
1314	.050	.0946
1322	.060	.0951

Specimen B 5

Strain Rate Cycled by I
($2.14 - 21.4 \times 10^{-4}$ sec^{-1})

σ (g/mm^2)	$\frac{\Delta\sigma}{\sigma_1}$	$\ln(1+\frac{\delta}{L_o})$
284	.193	.0035
323	.185	.0057
342	.213	.0062
365	.155	.0083
368	.203	.0089
392	.158	.0108
397	.180	.0110
400	.131	.0132
405	.161	.0138
431	.121	.0163
432	.160	.0167
455	.124	.0193
463	.141	.0197
487	.088	.0223
492	.141	.0227
512	.111	.0248
519	.128	.0252

Specimen B 15

Strain Rate Cycled by I
($2.14 - 21.4 \times 10^{-4}$ sec^{-1})

σ (g/mm^2)	$\frac{\Delta\sigma}{\sigma_1}$	$\ln(1+\frac{\delta}{L_o})$
252	.233	.0034
276	.165	.0054
286	.183	.0071
303	.145	.0089
313	.178	.0106
329	.154	.0123
341	.162	.0144
362	.130	.0163
418	.126	.0232
436	.101	.0250
450	.106	.0272
468	.095	.0290
478	.114	.0308
497	.090	.0327
507	.110	.0344
528	.086	.0362
542	.099	.0380
565	.076	.0401
580	.088	.0420
597	.077	.0438
610	.097	.0455
628	.076	.0472
646	.085	.0491
663	.071	.0507
682	.081	.0526
700	.070	.0548
723	.076	.0570
741	.062	.0589
764	.080	.0613
787	.062	.0632
806	.078	.0653
829	.063	.0671
850	.069	.0695
866	.058	.0705
880	.072	.0723
905	.065	.0741
931	.078	.0760
952	.064	.0778
971	.072	.0797
990	.064	.0814
1020	.067	.0835

Specimen B 16

Strain Rate Cycled by I
($2.14 - 214 \times 10^{-4}$ sec^{-1})

σ (g/mm^2)	$\frac{\Delta\sigma}{\sigma_1}$	$\ln(1+\frac{\delta}{L_o})$
370	.702	.0044
625	.212	.0227
633	.369	.0252
794	.173	.0329
824	.274	.0359

Specimen B 17

Strain Rate Cycled by I
($2.14 - 214 \times 10^{-4}$ sec^{-1})

σ (g/mm^2)	$\frac{\Delta\sigma}{\sigma_1}$	$\ln(1+\frac{\delta}{L_o})$
382	.682	.0036
586	.252	.0151
599	.403	.0176
802	.173	.0302
820	.236	.0333
1000	.149	.0477
1019	.210	.0504
1208	.130	.0626
1229	.193	.0659
1414	.124	.0780

Specimen B 18

Strain Rate Cycled by I
($2.14 - 214 \times 10^{-4}$ sec^{-1})

σ_1 (g/mm^2)	$\frac{\Delta\sigma}{\sigma_1}$	$\ln(1+\frac{\delta}{L_0})$
585	.239	.0216
615	.469	.0254
839	.186	.0357
880	.252	.0411
1330	.120	.0683

Specimen B 34

Strain Rate Cycled by II
($4.28 - 42.8 \times 10^{-4}$ sec^{-1})

σ_1 (g/mm^2)	$\frac{\Delta\sigma}{\sigma_1}$	$\ln(1+\frac{\delta}{L_0})$
396	.162	.0027
478	.096	.0088
488	.118	.0095
655	.067	.0176
683	.082	.0183
852	.058	.0270
894	.067	.0284
1041	.053	.0349

Specimen B 35

Strain Rate Cycled by II
($4.28 - 42.8 \times 10^{-4}$ sec^{-1})

σ_1 (g/mm^2)	$\frac{\Delta\sigma}{\sigma_1}$	$\ln(1+\frac{\delta}{L_0})$
230	.710	.0013
395	.121	.0110
406	.144	.0132
456	.107	.0213
464	.122	.0231
533	.095	.0347
546	.102	.0366
613	.083	.0472
626	.093	.0490
702	.077	.0607
720	.085	.0629
766	.078	.0695

Specimen B 26

Strain Rate Changed by III
($2.14 - 214 \times 10^{-4}$ sec^{-1})

σ_1 (g/mm^2)	$\Delta\sigma$ (g/mm^2)	$\ln(1+\frac{\delta}{L_0})$
306	189	.0131
429	125	.0224
493	38	.0317
703		.0405

Specimen B 29

Strain Rate 21.4 x 10^{-4} sec^{-1}
(decay and reload)

σ (g/mm^2)	$\Delta\sigma$ (g/mm^2)	$\ln(1+\frac{\delta}{L_o})$
498	5	.0090
557	6	.0182
597	10	.0244
656	11	.0319
695	12	.0358
770	13	.0439
845	9	.0514

Specimen B 28

Strain Rate 214 x 10^{-4} sec^{-1}
(relax and reload)

σ (g/mm^2)	$\Delta\sigma$ (g/mm^2)	$\ln(1+\frac{\delta}{L_o})$
624	81	.0205
1231	110	.0541

Specimen B 27

Strain Rate 21.4 x 10^{-4} sec^{-1}
(relax and reload)

σ (g/mm^2)	$\Delta\sigma$ (g/mm^2)	$\ln(1+\frac{\delta}{L_o})$
519		.0087
581	5	.0180
642	6	.0272
720	5	.0386
808	2	.0518
855		.0581

APPENDIX IV

Effect of Surface Removal on Mechanical Properties

Specimen B 12

Strain Rate 4.28×10^{-4} sec^{-1}
76 μ removed between changes

σ_1 (g/mm^2)	$\Delta\sigma$ (g/mm^2)	$\ln(1+\frac{\delta}{L_o})$
295	- 15	.0015
373	+ 15	.0295
521	+ 26	.0595
745	+ 59	.0955
931		.1029

Specimen B 11

Strain Rate Cycled by III
($2.14 - 21.4 \times 10^{-4}$ sec^{-1})
76 μ removed between changes

σ_1 (g/mm^2)	$\Delta\sigma$ (g/mm^2)	$\ln(1+\frac{\delta}{L_o})$
374	+ 38	.0005
553	+ 25	.0313
616	+ 112	.0406
950	- 30	.0646
1082	+ =68	.0812
2010		.1346

Specimen B 32

Strain Rate Cycled by III
($2.14 - 21.4 \times 10^{-4}$ sec^{-1})
76 μ removed between changes

σ_1 (g/mm^2)	$\Delta\sigma$ (g/mm^2)	$\ln(1+\frac{\delta}{L_o})$
405	70	.0065
463	103	.0207
607	111	.0336
798	19	.0484
923		.0632

Specimen B 30

Strain Rate Cycled by III
($2.14 - 21.4 \times 10^{-4}$ sec^{-1})
38 μ removed between changes

σ_1 (g/mm^2)	$\Delta\sigma$ (g/mm^2)	$\ln(1+\frac{\delta}{L_o})$
447	12	.0268
464	59	.0372
555	19	.0489
617	56	.0607
723	22	.0734
765	60	.0829
881	38	.0961
941	89	.1061
1109	13	.1206
1180		.1268

Specimen B 31

Strain Rate Cycled by III
($2.14 - 21.4 \times 10^{-4}$ sec^{-1})
38 μ removed between changes

σ_1 (g/mm^2)	$\Delta\sigma$ (g/mm^2)	$\ln(1+\frac{\delta}{L_o})$
381	8	.0105

Specimen B 24

Strain Rate Cycled by III
($2.14 - 214 \times 10^{-4}$ sec^{-1})
76 removed between changes

σ_1 (g/mm^2)	$\Delta\sigma$ (g/mm^2)	$\ln(1+\frac{\delta}{L_o})$
470	106	.0137
515	145	.0194
645	105	.0326
690	32	.0387
945		.0650

Specimen B 23

Strain Rate Cycled by III
($2.14 - 214 \times 10^{-4}$ sec^{-1})
76 removed between changes

σ_1 (g/mm^2)	$\Delta\sigma$ (g/mm^2)	$\ln(1+\frac{\delta}{L_o})$
341	154	.0140

APPENDIX V

Properties of Coated Specimens

Tested at 4.3×10^{-4} sec^{-1}

Specimen Number	Temperature (°C)	Diffusion Time (hrs)	Layer Thickness (μ)	Yield Stress (g/mm^2)	Critical Tensile Stress (g/mm^2)	Ultimate Tensile Stress (g/mm^2)	Total Strain	Work-Hardening Slope ($g/mm^2 \times 10^{-4}$)
11	500*	41	12	450	570	673	.0205	.860
15	500*	50	47	675	1000	1000		
16	500*	24	18	471	750	845	.0098	.970
18	500*	12	15	365	580	775	.0160	1.22
20	500*	41	137	1700	1970	1970		
22	500*	41	150	1860		1860		
24	500*	41	160	1920		1920		
25	500*	20	125	1880		1880		
26	500*	11	91	1290	1700	1700		
28	500*	20	144	1670	2320	2320		
35	510*	21	47	760	880	975	.0051	1.51
55	421	11	30	270	297	339	.0102	.411
56	376	18	22	353	425	506	.0062	1.32
57	405	20	20	230	424	575	.0189	.800
58	422	20	30	444	517	580	.0089	.712
60	485	21	50	411	466	529	.0036	1.76
61	485	18	94	901	953	970		
64	590	18	27	310	481	535	.0091	.595
66	422	14	5	296	322	434	.0264	.425
69	485	21	91	1000	1140	1210	.0026	2.68
70	433	25	34	470	612	1087	.0210	2.26
71	440	18	38	340	361	495	.0116	1.15
72	590	18	69	806	873	873		
73	433	25	25	474	621	621		
74	422	14	10	344	395	578	.0212	.87
77	433	25	37	362	543	550	.0182	.38
81**	410	21	63	640	779	779		
82	410	21	45	413	624	624		

Specimen Number	Temperature (°C)	Diffusion Time (hrs)	Layer Thickness (μ)	Yield Stress (g/mm^2)	Critical Tensile Stress (g/mm^2)	Ultimate Tensile Stress (g/mm^2)	Total Strain	Work-Hardening Slope ($g/mm^2 \times 10^{-4}$)
83**	410	21	35	325	390	390		
84	410	21	46	644	700	700		
85**	582	4	105	1164	1290	1300		
87	582	4	107	1164	1385	1505	.0055	2.16
88	582	4	85	1050	1185	1215	.0021	1.45
89	536	3	3	230	264		.0573	.352
90	536	3	5	269	285		.0445	.351

Note: * — Temperature not known more accurately than ± 15°C

** — One face abraded. Given 20 strokes on 4/0 polishing paper.

APPENDIX VI

Representative X-ray data
CuK_{α} radiation, Ni Filter

Powder ground from specimen #20

Line#	Θ	$(hkl)_{cubic}$	Parameter (Å)
1	19.30	(111)	(Film shrinkage correction applied)
2	22.45	(200)	
3	32.71	(220)	
4	39.32	(311)	
5	40.81	(222)	
6	69.65	(422)	
7	59.00	(420)	4.023
8	50.15	(400)	4.020

Powder ground from specimen #24

1	19.31	(111)	
2	22.46	(200)	
3	32.73	(220)	
4	39.33	(311)	
5	41.43	(222)	
6	69.85	(422)	
7	59.03	(420)	4.020
8	50.13	(400)	4.021

Powder ground from specimen #18

1	19.34	(111)	
2	22.70	(200)	
3	32.95	(220)	
4	38.89	(311)	
5	40.35	(222)	
6	69.85	(422)	
7	59.00	(420)	4.022
8	50.18	(400)	4.021

Coating from specimen #29

Line#	θ	$(hkl)_{tetragonal}$	Parameter (Å)
1	30.06		
2	33.07	(110)	c = 4.64a = 3.06
3	50.62	(200)	c = 4.66a = 3.07
4	59.39	(103)	c = 4.69a = 3.08
5	64.72	(211)	c = 4.67a = 3.07
6	70.71	(113)	

Coating from specimen #34

1	30.01		
2	32.85	(110)	c = 4.68a = 3.07
3	50.48	(200)	c = 4.67a = 3.08
4	53.12	(103)	
5	55.75		
6	59.20		
7	64.55	(211)	c = 4.69a = 3.10
8	70.52	(113)	